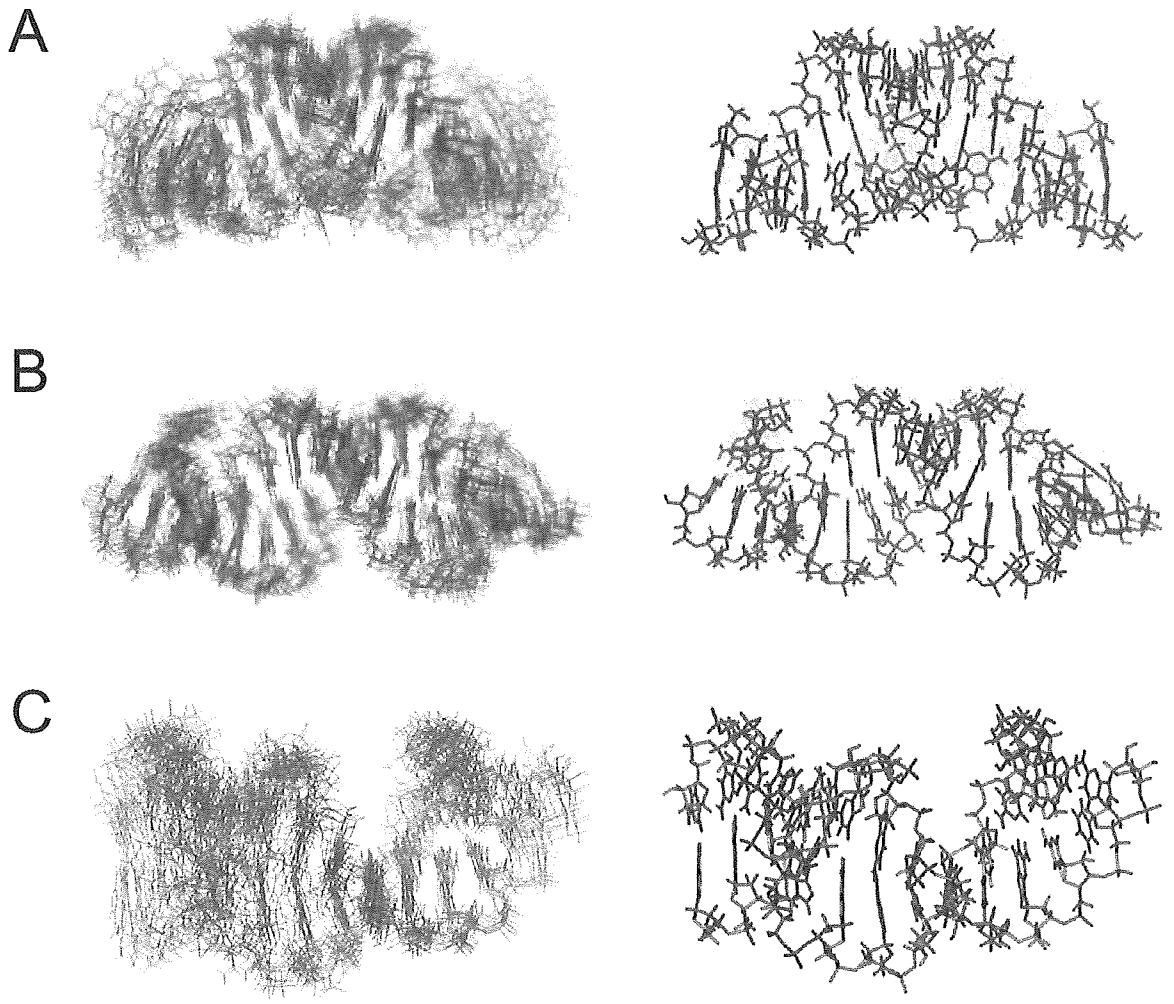

Fig. 4. **Solution structures of each part of DIS39.** Left panels show the superimposition of the 10 lowest energy structures and the right panels show the minimized average structures. (A) The loop region of loop25, as shown by the broken box in Fig. 1b, in the kissing-loop dimer. Each strand is colored in red or blue. (B) The loop region of loop25 in the extended-duplex dimer. (C) The stem-bulge-stem region of bulge34.

the kissing-loop dimer. The present structure is similar to the crystal structures in general, except for A15 and A16. In the present structure, A15 stacks on G14 and A16 interacts with the same residue in the other molecule (Fig. 6A, right). On the other hand, in the crystal structure, A15 and G16 are flipped out (*20*). It is noted that the numbering system of DIS39 is used for other structures for convenience, and position 16 is occupied by A or G depending on the strain. A15 and A16 (or G16) might be flexible and can be flipped out even in solution. Mujeeb *et al.* (*19*) determined the solution structure of the kissing-loop dimer. In this structure, A16 interacts with A15 and C24 in the other molecule, and, as a result, the distance between the two stems is relatively short. Thus, this restricted interaction makes the global structure different from the present structure and the crystal structure. However, the location of A15 is similar in the two solution structures. The difference in the conformation of A16 between the two solution structures may reflect the difference in the sequence of the stem adjacent to the loop and/or in the sample condition, including the salt concentration. The NOE connectivity determined in the present study agrees in general with those of Dardel *et al.* who analyzed the structure of the stem-loop region in the kissing-loop dimer by NMR (*34*).

Girard *et al.* (*21*) and Mujeeb *et al.* (*22*) determined the solution structures of extended-duplex dimers. In these two structures, as well as in the present structure, A15, A16 and A23 form a zipper like structure (Fig. 6B, right). On the other hand, in the case of the crystal structure of the extended-duplex dimer, G16 forms a G:A base pair and A15 is flipped out, and it was assumed that this in-out bulge transconformation is magnesium-dependent (*23*).

Structures of the stem-bulge-stem region were shown by Lawrence *et al.* (*26*) and Yuan *et al.* (*27*). In the solution structure determined by Lawrence *et al.* (*26*), continuous stackings were formed for each strand, G6-C8 and

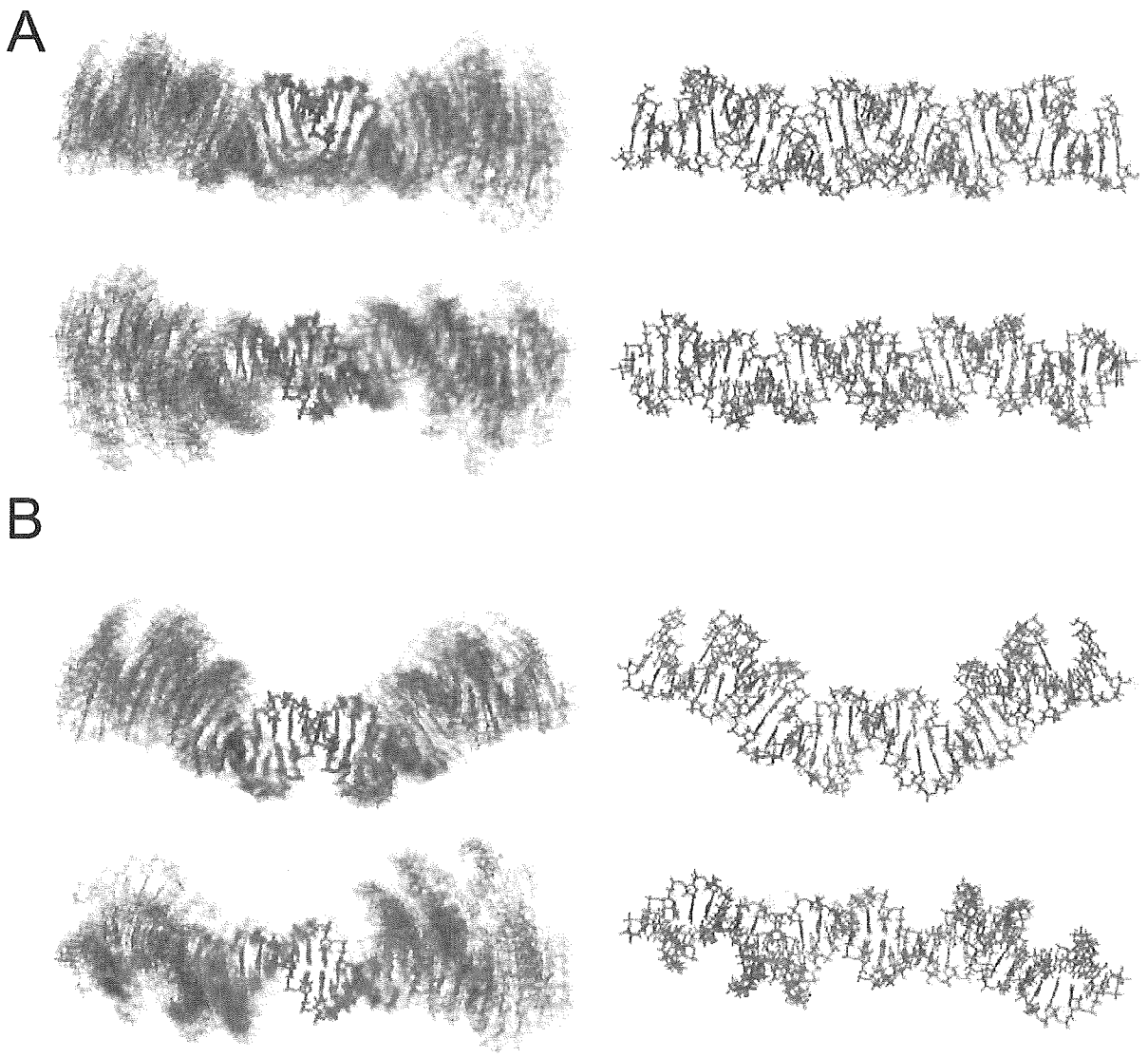

Fig. 5. **Solution structures of the (A) kissing-loop and (B) extended-duplex dimers of DIS39.** Left panels show the structures constructed by combining the structures of the loop (the 10 lowest energy structures of the kissing-loop or extended-duplex dimers) and the stem-bulge-stem (minimized average structure) regions. Right panels show the structures constructed by combining the minimized average structures of the loop and stem-bulge-stem regions. The two regions were combined by superimposing two base pairs, C12–G26 and U13–G25 (Fig. 1, gray area). Each strand is colored in red or blue and views from two different directions are shown.

G30-C34. Yuan *et al.* (*27*) showed that G7 and A31 form a base pair, and that G33 is not always stacked on G32 or C34, and, in general, the present structure is identical to the latter structure. Greatorex *et al.* (*25*) showed that the bulge region is too flexible to determine the conformation. These conformational differences may be caused by differences in the stability of the terminal stem. Lawrence *et al.* (*26*) adopted a stable 7 base-pair stem, and their structure forms an ordered conformation in the bulge region. In contrast, Greatorex *et al.* (*25*) adopted an unstable 4 base-pair stem and the bulge region is flexible. Yuan *et al.* (*27*) adopted a 4 base-pair stem and a flanking adenosine residue at the 3′ terminal that must stabilize the stem. In the present study, a 6 base-pair stem was used.

Mechanism of the Two Stem Dimerization—Between the kissing-loop and extended-duplex dimers, A16 shows the most drastic change in interaction with other residues, suggesting that A16 is the key residue in the two step dimerization reaction. The difference in the A16 conformation among structures with different sequences and determined under different conditions as described above, also suggests the importance of this residue. Mujeeb *et al.* (*19, 22*) also pointed out the flexibility around the junction of the loop and the stem of DIS in the kissing-loop and

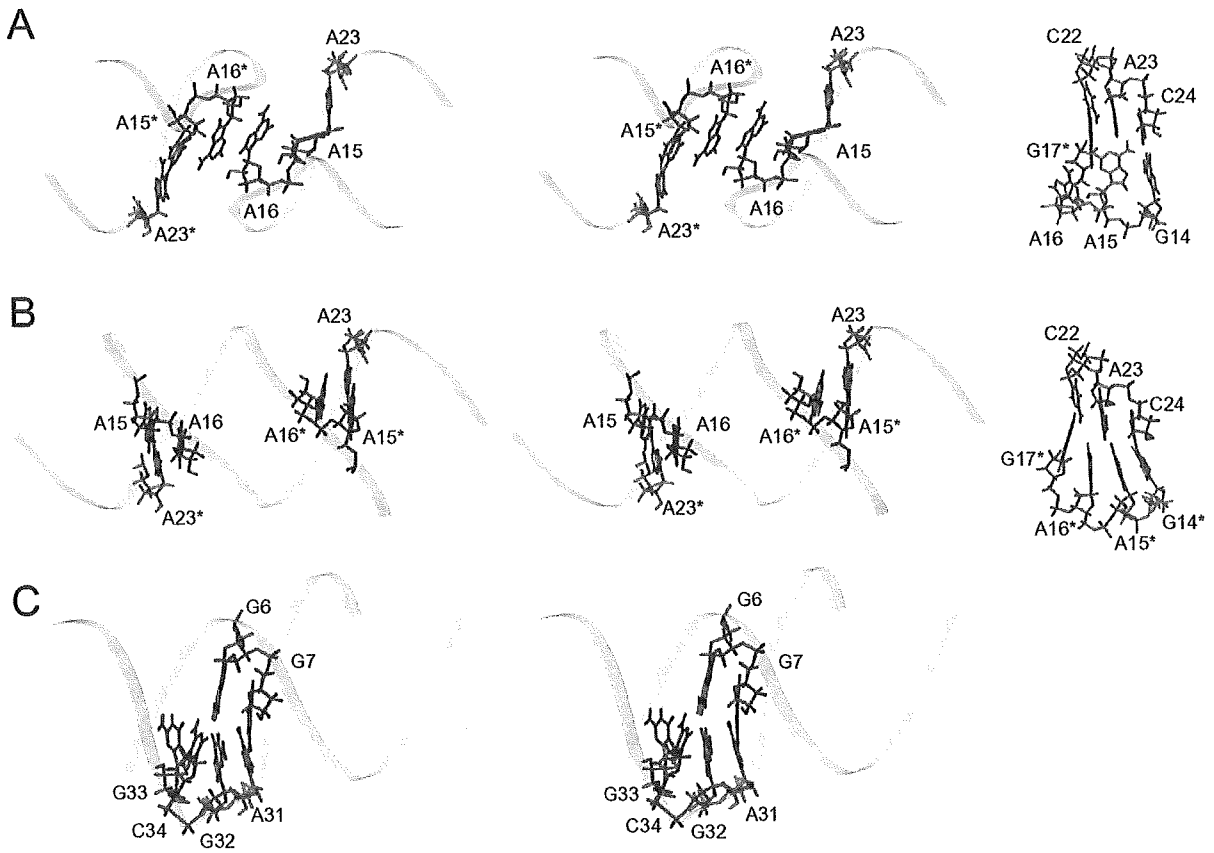

Fig. 6. **Structures of the linking regions.** (A) Regions linking the stem and loop in the kissing-loop dimer. The left panels show the positions of A15, A16, and A23 in the entire structure in a stereo view, and the right panels show residues linking the stem and loop. Asterisks indicate residues in the other strand. (B) Regions linking the stem and loop in the extended-duplex dimer. (C) The bulge region linking the two stems.

extended-duplex dimers. Imino proton signals due to U9:A29 and U10:A28 are much broader than other signals in the stem region, and no imino proton signal due to C8:G30 was observed. Thus, the stem between the loop and bulge is destabilized by the bulge region. Our previous experiments also showed that the bulge region is required for the two-step dimerization to adjust the thermal stability of DIS, and Greatorex *et al.* (*25*) also indicated that the flexibility of the bulge region is critical based on the fact that mutations in the bulge region strongly affect the melting temperature, as well as the fact that none of the wild-type sequences in the bulge region that increase the melting temperature is ever found in wild-type viruses. Thus, the conformational conversion from the kissing-loop dimer to the extended-duplex dimer might require two factors, the movement of A16 and the modest stability of the stem caused by the presence of the bulge region.

In the present study, a set of structures corresponding to the initial and final structures of the two-step dimerization of DIS are provided; these structures will promote studies to elucidate the molecular mechanism of the conformational change in the two-step dimerization, including an analysis of the interaction between DIS and NCp7, in addition to the molecular dynamics approach.

Coordinates: The structure has been deposited in the Protein Data Bank (accession code 2D17: the stem-bulge-stem region of bulge34, 2D18: the extended-duplex dimer of loop25, 2D19: the kissing-loop dimer of loop25, 2D1A: the extended-duplex dimer of DIS39 and 2D1B: the kissing-loop dimer of DIS39).

This work was supported by the "Research for the Future" Program (JSPS-RFTF97L00503) from the Japan Society for the Promotion of Science, and, in part, by a Grant-in-Aid for High Technology Research from the Ministry of Education, Science, Sports and Culture, Japan.

REFERENCES

1. Hoglund, S., Ohagen, A., Goncalves, J., Panganiban, A.T., and Gabuzda, D. (1997) Ultrastructure of HIV-1 genomic RNA. *Virology* **233**, 271–279
2. Laughrea, M., Jette, L., Mak, J., Kleiman, L., Liang, C., and Wainberg, M.A. (1997) Mutations in the kissing-loop hairpin of human immunodeficiency virus type 1 reduce viral infectivity as well as genomic RNA packaging and dimerization. *J. Virol.* **71**, 3397–3406
3. Clever, J.L. and Parslow, T.G. (1997) Mutant human immunodeficiency virus type 1 genomes with defects

in RNA dimerization or encapsidation. *J. Virol.* **71**, 3407–3414
4. Paillart, J.C., Berthoux, L., Ottmann, M., Darlix, J.L., Marquet, R., Ehresmann, B., and Ehresmann, C. (1996) A dual role of the putative RNA dimerization initiation site of human immunodeficiency virus type 1 in genomic RNA packaging and proviral DNA synthesis. *J. Virol.* **70**, 8348–8354
5. Laughrea, M. and Jette, L. (1994) A 19-nucleotide sequence upstream of the 5′ major splice donor is part of the dimerization domain of human immunodeficiency virus 1 genomic RNA. *Biochemistry* **33**, 13464–13474
6. Skripkin, E., Paillart, J.C., Marquet, R., Ehresmann, B., and Ehresmann, C. (1994) Identification of the primary site of the human immunodeficiency virus type 1 RNA dimerization *in vitro*. *Proc. Natl. Acad. Sci. USA* **91**, 4945–4949
7. Fu, W. and Rein, A. (1993) Maturation of dimeric viral RNA of Moloney murine leukemia virus. *J. Virol.* **67**, 5443–5449
8. Fu, W., Gorelick, R.J., and Rein, A. (1994) Characterization of human immunodeficiency virus type 1 dimeric RNA from wild-type and protease-defective virions. *J. Virol.* **68**, 5013–5018
9. Laughrea, M. and Jette, L. (1996) Kissing-loop model of HIV-1 genome dimerization: HIV-1 RNAs can assume alternative dimeric forms, and all sequences upstream or downstream of hairpin 248–271 are dispensable for dimer formation. *Biochemistry* **35**, 1589–1598
10. Muriaux, D., Fosse, P., and Paoletti, J. (1996) A kissing complex together with a stable dimer is involved in the HIV- 1Lai RNA dimerization process *in vitro*. *Biochemistry* **35**, 5075–5082
11. Muriaux, D., Girard, P.M., Bonnet-Mathoniere, B., and Paoletti, J. (1995) Dimerization of HIV-1Lai RNA at low ionic strength. An autocomplementary sequence in the 5′ leader region is evidenced by an antisense oligonucleotide. *J. Biol. Chem.* **270**, 8209–8216
12. Laughrea, M., Shen, N., Jette, L., Darlix, J., Kleiman, L., and Wainberg, M.A. (2001) Role of distal zinc finger of nucleocapsid protein in genomic RNA dimerization of human immunodeficiency virus type 1; No role for the palindrome crowning the R-U5 hairpin. *Virology* **281**, 109–116
13. de Guzman, R.N., Wu, Z.R., Stalling, C.C., Pappalardo, L., Borer, P.N., and Summers, M.F. (1998) Structure of the HIV-1 nucleocapsid protein bound to the SL3 ψ–RNA recognition element. *Science* **279**, 384–388
14. Amarasinghe, G.K., de Guzman, R.N., Turner, B.G., Chancellor, K.J., Wu, Z.R., and Summers, M.F. (2000) NMR structure of the HIV-1 nucleocapsid protein bound to Stem-Loop SL2 of the ψ–RNA packaging signal. Implications for Genome recognition. *J. Mol. Biol.* **301**, 491–511
15. Berkowitz, R., Fisher, J., and Goff, S.P. (1996) RNA packaging. *Curr. Top. Microbiol. Immunol.* **214**, 177–218
16. Darlix, J.L., Lopez-Lastra, M., Mély, Y., and Roques, B. (2003) Nucleocapsid protein chaperoning of nucleic acids at the heart of HIV structure, assembly and cDNA synthesis. In *HIV Sequence Compendium 2002* (Kuiken, C., Foley, B., Freed, E., Hahn, B., Marx, P., McCutchan, F., Mellors, J.W., Wolinsky, S., and Korber, B., eds.) pp. 69–88, Los Alamos National Laboratory, Los Alamos, NM
17. Takahashi, K., Baba, S., Koyanagi, Y., Yamamoto, N., Takaku, H., and Kawai, G. (2001) Two basic regions of NCp7 are sufficient for conformational conversion of HIV-1 dimerization initiation site from kissing-loop dimer to extended-duplex dimer. *J. Biol. Chem.* **276**, 31274–31278
18. Baba, S., Takahashi, K., Koyanagi, Y., Yamamoto, N., Takaku, H., Gorelick, R.J., and Kawai, G. (2003) Role of the Zinc Fingers of HIV-1 Nucleocapsid Protein in Maturation of Genomic RNA. *J. Biochem.* **134**, 637–639
19. Mujeeb, A., Clever, J.L., Billeci, T.M., James, T.L., and Parslow, T.G. (1998) Structure of the dimer initiation complex of HIV-1 genomic RNA. *Nat. Struct. Biol.* **5**, 432–436
20. Ennifar, E., Walter, P., Ehresmann, B., Ehresmann, C., and Dumas, P. (2001) Crystal Structures of Coaxially-Stacked Kissing Complexes of the HIV-1 RNA Dimerization Initiation Site. *Nat. Struct. Biol.* **8**, 1064–1068
21. Girard, F., Barbault, F., Gouyette, C., Huynh-Dinh, T., Paoletti, J., and Lancelot, G. (1999) Dimer Initiation Sequence of HIV-1Lai Genomic RNA: NMR Solution Structure of the Extended Duplex. *J. Biomol. Struct. Dyn.* **16**, 1145–1157
22. Mujeeb, A., Parslow, T.G., Zarrinpar, A., Das, C., and James, T.L. (1999) NMR structure of the mature dimer initiation complex of HIV-1 genomic RNA. *FEBS Lett.* **458**, 387–392
23. Ennifar, E., Yusupov, M., Walter, P., Marquet, R., Ehresmann, B., Ehresmann, C., and Dumas, P. (1999) The crystal structure of the dimerization initiation site of genomic HIV-1 RNA reveals an extended duplex with two adenine bulges. *Structure Fold Des.* **7**, 1439–1449
24. Ennifar, E., Walter, P., and Dumas, P. (2003) A Crystallographic Study of the Binding of 13 Metal Ions to Two Related RNA Duplexes. *Nucleic Acids Res.* **31**, 2671–2682
25. Greatorex, J., Gallego, J., Varani, G., and Lever, A. (2002) Structure and Stability of Wild-Type and Mutant RNA Internal Loops from the SL-1 Domain of the HIV-1 Packaging Signal. *J.Mol.Biol.* **322**, 543–557
26. Lawrence, D.C., Stover, C.C., Noznitsky, J., Wu, Z., and Summers, M. F. (2003) Structure of the Intact Stem and Bulge of HIV-1 Psi-RNA Stem-Loop Sl1. *J. Mol. Biol.* **326**, 529–542
27. Yuan, Y., Kerwood, D.J., Paoletti, A.C., Shubsda, M.F., and Borer, P.N. (2003) Stem of SL1 RNA in HIV-1: structure and nucleocapsid protein binding for a 1 × 3 internal loop. *Biochemistry* **42**, 5259–5269
28. Shen, N., Jette, L., Liang, C., Wainberg, M.A., and Laughrea, M. (2000) Impact of human immunodeficiency virus type 1 RNA dimerization on viral infectivity and of stem-loop B on RNA dimerization and reverse transcription and dissociation of dimerization from packaging. *J. Virol.* **74**, 5729–5735
29. Takahashi, K.I., Baba, S., Chattopadhyay, P., Koyanagi, Y., Yamamoto, N., Takaku, H., and Kawai, G. (2000) Structural requirement for the two-step dimerization of human immunodeficiency virus type 1 genome. *RNA* **6**, 96–102
30. Varani, G., Aboul-era, F., and Allain, F.H.-T. (1996) NMR investigation of RNA structure. *Prog. NMR Spect.* **29**, 51–127
31. Takahashi, K., Baba, S., Hayashi, S., Koyanagi, Y., Yamamoto, N., Takaku, H., and Kawai, G. (2000) NMR analysis on intra- and inter-molecular stems in the dimerization initiation site of the HIV-1 genome. *J. Biochem.* **127**, 681–639
32. St.Louis, D.C., Gotte, D., Sanders-Buell, E., Ritchey, D.W., Salminen, M.O., Carr, J.K., and McCutchan, F.E. (1998) Infectious molecular clones with the nonhomologous dimer initiation sequences found in different subtypes of human immunodeficiency virus type 1 can recombine and initiate a spreading infection in vitro. *J. Virol.* **72**, 3991–3998
33. Weixlbaumer, A., Werner, A., Flamm, C., Westhof, E., and Schroeder, R. (2004) Determination of thermodynamic parameters for HIV DIS type loop-loop kissing complexes. *Nucleic Acids Res.* **32**, 5126–5133
34. Dardel, R., Marguet, R., Ehresmann, C., Ehresmann, B., and Blanquet, S. (1998) Solution studies of the dimerization initiation site of HIV-1 genomic RNA. *Nucleic Acids Res.* **26**, 3567–3571

JOURNAL OF VIROLOGY, Mar. 2005, p. 2847–2858 Vol. 79, No. 5
0022-538X/05/$08.00+0 doi:10.1128/JVI.79.5.2847–2858.2005

Involvement of the Toll-Like Receptor 9 Signaling Pathway in the Induction of Innate Immunity by Baculovirus†

Takayuki Abe,[1] Hiroaki Hemmi,[2] Hironobu Miyamoto,[1] Kohji Moriishi,[1] Shinichi Tamura,[3] Hiroshi Takaku,[4] Shizuo Akira,[2] and Yoshiharu Matsuura[1]*

Research Center for Emerging Infectious Diseases,[1] Department of Host Defense,[2] and Laboratory of Prevention of Viral Diseases,[3] Research Institute for Microbial Diseases, Osaka University, Osaka, and Department of Industrial Chemistry and High Technology Research Center, Chiba Institute of Technology, Chiba,[4] Japan

Received 11 July 2004/Accepted 6 October 2004

We have previously shown that mice inoculated intranasally with a wild-type baculovirus (*Autographa californica* nuclear polyhedrosis virus [AcNPV]) are protected from a lethal challenge by influenza virus. However, the precise mechanism of induction of this protective immune response by the AcNPV treatment remained unclear. Here we show that AcNPV activates immune cells via the Toll-like receptor 9 (TLR9)/MyD88-dependent signaling pathway. The production of inflammatory cytokines was severely reduced in peritoneal macrophages (PECs) and splenic CD11c$^+$ dendritic cells (DCs) derived from mice deficient in MyD88 or TLR9 after cultivation with AcNPV. In contrast, a significant amount of alpha interferon (IFN-α) was still detectable in the PECs and DCs of these mice after stimulation with AcNPV, suggesting that a TLR9/MyD88-independent signaling pathway might also participate in the production of IFN-α by AcNPV. Since previous work showed that TLR9 ligands include bacterial DNA and certain oligonucleotides containing unmethylated CpG dinucleotides, we also examined the effect of baculoviral DNA on the induction of innate immunity. Transfection of the murine macrophage cell line RAW264.7 with baculoviral DNA resulted in the production of the inflammatory cytokine, while the removal of envelope glycoproteins from viral particles, UV irradiation of the virus, and pretreatment with purified baculovirus envelope proteins or endosomal maturation inhibitors diminished the induction of the immune response by AcNPV. Together, these results indicate that the internalization of viral DNA via membrane fusion mediated by the viral envelope glycoprotein, as well as endosomal maturation, which releases the viral genome into TLR9-expressing cellular compartments, is necessary for the induction of the innate immune response by AcNPV.

The baculovirus *Autographa californica* nuclear polyhedrosis virus (AcNPV) has long been used as a biopesticide and as an efficient tool for recombinant protein production in insect cells (39, 42). Subsequently, its efficacy for the delivery of high-level expression of foreign genes under the control of mammalian promoters in infected mammalian cells was also demonstrated (12, 26, 48). Since it causes no visible cytopathic effects, even at high titers, and does not replicate in mammalian cells (49), this baculovirus is now recognized as a useful viral vector, not only for the expression of foreign proteins in insect cells, but also for gene delivery to mammalian cells (4, 9, 12, 16, 26, 28, 37, 45, 48, 49, 53, 54).

AcNPV was also shown to be capable of stimulating interferon (IFN) production in mammalian cell lines and can confer protection from lethal encephalomyocarditis virus infections in mice (18). We demonstrated that intranasal inoculation with AcNPV induces a strong innate immune response and protects mice from a lethal challenge of influenza A and B viruses (1). Furthermore, inoculation with baculovirus induces the secretion of inflammatory cytokines, such as tumor necrosis factor alpha (TNF-α), interleukin-6 (IL-6), and IL-12, in RAW264.7, a murine macrophage cell line. However, the precise mechanism of induction of the protective immune response by a pretreatment with AcNPV remained unclear.

Members of the IL-1 receptor/Toll-like receptor (TLR) superfamily are key mediators of innate and adaptive immunity (5). Toll, the first member of this superfamily to be identified, was initially discovered as a factor involved in dorsoventral axis formation in fly embryos and was later shown to participate in host defense mechanisms (38). A family of TLRs exists in mammals and has been shown to play an important role not only in the recognition of a wide variety of infectious pathogens and their products, but also in protection of the host from infections with pathogens. So far, 11 TLR family members and their corresponding ligands have been identified, with TLR1 being the only orphan receptor among them. Different TLRs have been shown to mediate immune responses to a variety of different pathogen-derived elements. For example, TLR4, TLR5, and TLR9 are essential for the recognition of lipopolysaccharides (LPS), bacterial flagellin, and bacterial DNA containing unmethylated CpG motifs, respectively (21, 24, 27, 46). TLR2 is implicated in the recognition of peptidoglycan (PGN) and lipopeptides (7, 13, 50, 57), while TLR6 can associate with TLR2 and recognize PGN and lipopeptides derived from mycoplasma (44). On the other hand, TLR3 has been shown to activate immune cells in response to virus-derived double-stranded RNA (6). Although synthetic imidazoquinoline com-

* Corresponding author. Mailing address: Research Center for Emerging Infectious Diseases, Research Institute for Microbial Diseases, Osaka University, 3-1 Yamada-oka, Suita, Osaka 565-0871, Japan. Phone: 81-6-6879-8340. Fax: 81-6-6879-8269. E-mail: matsuura@biken.osaka-u.ac.jp.

† This study is dedicated to the memory of Ikuko Yanase.

pounds and guanosine analogs with antiviral activities have been shown to activate TLR7 and TLR8 (25, 36), it was recently demonstrated that single-stranded RNAs from RNA viruses are the natural ligands of these receptors (17, 23). The most recently identified TLR, termed TLR11, senses bacteria that cause infections of the bladder and kidney (60). In summary, TLRs recognize specific components derived from pathogens and activate a signaling cascade that causes proinflammatory cytokine production and subsequent immune responses.

TLRs share a common cytoplasmic Toll–IL-1 receptor (TIR) domain. MyD88, also a TIR domain-containing protein, associates with TLRs and acts as an adapter that recruits IL-1 receptor-associated kinase and TNF receptor-associated factor 6 (TRAF6) to TLRs. Macrophages isolated from MyD88-deficient mice fail to activate NF-κB and Jun N-terminal protein kinase or to produce inflammatory cytokines in response to microbial components such as lipopeptides, LPS, and CpG-rich bacterial DNA (20, 52), indicating that MyD88 is a critical component in the signaling pathway that leads to the production of inflammatory cytokines.

Viruses are obligate intracellular parasites; accordingly, viral proteins synthesized in host cells bear modifications that reflect the identity and characteristics of the host. Therefore, viral particles do not display exclusively pathogen-associated molecular patterns. Although the mechanisms by which the innate immune response is induced by viral infection are poorly understood, there is increasing evidence suggesting that TLRs function to detect viruses and trigger inflammatory responses. For instance, respiratory syncytial virus and mouse mammary tumor virus activate innate immunity through TLR4 (22, 34, 47), which is a signaling receptor for LPS. Similarly, hemagglutinin from wild-type measles virus was reported to activate TLR2 (10), which also recognizes certain elements of gram-positive bacteria and fungi. Herpes simplex virus type 1 (HSV-1) and human cytomegalovirus have also been shown to recognize TLR2 (15, 35), while vaccinia virus encodes proteins containing amino acid sequences similar to the Toll/IL-1 receptor domain and inhibits IL-1-, IL-18-, and TLR4-mediated signal transduction (11).

It was recently shown that HSV-1 and -2, whose genomes contain abundant CpG motifs, can induce angiogenesis and a variety of diseases, including herpes stromal keratitis, that produce chronic inflammatory responses via a TLR9/MyD88-dependent signaling pathway (33, 40, 61). HSV-1 and -2 are also able to trigger alpha interferon (IFN-α) secretion from plasmacytoid dendritic cells through TLR9/MyD88-dependent signaling (33, 40). The TLR9-mediated recognition of HSV by immunocompetent cells suggests that this recognition pathway may be important for the recognition of other DNA viruses.

For this study, we characterized the innate immune response induced by AcNPV. Peritoneal macrophages and splenic $CD11c^+$ dendritic cells obtained from TLR9 or MyD88 knockout mice exhibited severe reductions in proinflammatory cytokine production following stimulation with AcNPV, whereas a significant amount of IFN-α was still detectable in these cells. In addition, the frequency of CpG motifs in the AcNPV genome was similar to that of bacterial DNA and significantly higher than that of mammalian DNA. Furthermore, stimulation by AcNPV was eliminated by a treatment with inhibitors of endosomal acidification. These results indicate that the internalization of viral AcNPV DNA via membrane fusion by envelope glycoproteins found in the endosome is required for the induction of a TLR9/MyD88-dependent innate immune response.

MATERIALS AND METHODS

Mice and cell culture. C57BL/6 mice were purchased from Clea Japan, Inc., Tokyo, Japan. MyD88-deficient ($MyD88^{-/-}$) mice were established as previously described (2) and backcrossed more than eight times with C57BL/6 mice. $TLR9^{-/-}$ mice were generated as previously described (24). The mice were injected intraperitoneally with 2 ml of 4% thioglycolate (Sigma-Aldrich Co., St. Louis, Mo.), and cells were harvested 3 days later by peritoneal lavage. The mouse macrophage cell line RAW264.7 was purchased from Riken Cell Bank (Tsukuba, Japan) and maintained in Dulbecco's modified Eagle's medium (Sigma-Aldrich) supplemented with 10% (vol/vol) heat-inactivated fetal calf serum (FCS), 1.5 mM L-glutamine, 100 U of penicillin/ml, and 100 μg of streptomycin/ml at 37°C in a 5% CO_2 humidified incubator.

Viruses and reagents. AcNPV was propagated in *Spodoptera frugiperda* (Sf-9) cells in Sf-900II insect medium supplemented with 10% (vol/vol) heat-inactivated FCS. A mutant baculovirus, AcNPVΔ64, which lacks the gp64 envelope protein and possesses the green fluorescent protein gene under the control of the polyhedrin promoter in the gp64 gene locus, was generated (Y. Kitagawa et al., unpublished data). AcNPV and AcNPVΔ64 were purified as previously described (1). The inactivation of AcNPV was performed with a Stratalinker 2400 (Stratagene, La Jolla, Calif.) using short-wavelength UV radiation (UVC, 254 nm) at a distance of 5 cm for 30 min on ice (1.6×10^4 mJ/cm^2). The inactivation of infectivity was verified by a plaque assay with Sf-9 cells.

AcNPV DNA was isolated from the purified virions by a treatment with 10 mg of proteinase K (Sigma-Aldrich)/ml and 10% sodium dodecyl sulfate (SDS) in sterile phosphate-buffered saline (PBS) for 2 h at 55°C. The viral DNA was purified by phenol-chloroform-isoamyl alcohol extraction, precipitated at 12,000 × *g*, and resuspended in sterile endotoxin-free Tris-buffered saline. RNAs were removed by incubation with RNase A (10 mg/ml) (Wako Pure Chemical Industries, Osaka, Japan) for 1 h at 37°C, and the viral DNA was extracted as described above. The resultant DNA exhibited a single band by electrophoresis, and neither protein nor chromosomal DNA of insect cells was detected.

Phosphorothioate-stabilized mouse CpG (mCpG) oligodeoxynucleotides (ODN1668) (TCC-ATG-ACG-TTC-CTG-ATG-CT) and human CpG (hCpG) oligodeoxynucleotides (ODN2006) (TCG-TCG-TTT-TGT-CGT-TTT-GTC-GTT) were purchased from Invitrogen (Tokyo, Japan). Guanosine, 2′-deoxy-G, 8-bromo-G, 7-methyl-G, 7-allyl-8-oxo-G (loxoribine) was purchased from Invivogen (San Diego, Calif.). LPS derived from *Salmonella enterica* serovar Minnesota (Re-595), PGN derived from *Staphylococcus aureus*, monodansylcadaverine (MDC), and chloroquine were purchased from Sigma-Aldrich. Bafilomycin A1 and ammonium chloride were purchased from Wako Pure Chemical Industries. An anti-p39 mouse monoclonal antibody was kindly provided by G. F. Rohrmann. The virus stocks and the other TLR ligands were free of endotoxin (<0.01 endotoxin units/ml), as determined by use of a Pyrodick endotoxin measure kit (Seikagaku Co., Tokyo, Japan).

Production of authentic and truncated forms of gp64 proteins. cDNAs encoding a deletion mutant of gp64 lacking the transmembrane region (gp64ΔTM) as well as a wild-type version of gp64 were obtained by PCRs with AcNPV DNA as a template. The same 5′ primer (5′-CATAAGCTTATGGTAAGCGCTATT GTTTTATAT-3′) was used to amplify the gp64 and gp64ΔTM cDNAs, and the 3′ primers were 5′-GATTCTAGAATATATTGTCTATTACGGTTTCT-3′ and 5′ GATTCTAGAATCGAAGTCAATTTAGCGGCCAA-3′, respectively. cDNAs were subcloned into HindIII and XbaI sites in pIB/V5-His (Invitrogen). The sequences of the recombinant plasmids, pIBgp64/V5-His and pIBgp64ΔTM/V5-His, were confirmed by DNA sequencing. These plasmids were transfected into Sf-9 cells by the use of Unifector (B-Bridge International, Inc., San Jose, Calif.). After 3 days of incubation, the recombinant gp64 proteins were purified from cell lysates or supernatants by use of a column of nickel-nitrilotriacetic acid beads (QIAGEN, Valencia, Calif.). The protein concentrations were determined by use of a Micro BCA protein assay kit (Pierce, Rockford, Ill.). The recombinant proteins were analyzed by SDS–12.5% polyacrylamide gel electrophoresis (SDS–12.5% PAGE) under reducing conditions, stained with GelCord Blue staining reagent (Pierce), and detected by immunoblotting analysis with an antihexahistidine monoclonal antibody (Santa Cruz Biotechnology, Santa Cruz, Calif.).

Isolation of peritoneal cells and cytokine production. To evaluate cytokine production from macrophages in vitro, we seeded thioglycolate-elicited perito-

neal cells (PECs) into 96-well plates at a concentration of 2×10^5 cells/well and stimulated them with various doses of AcNPV and loxoribine. After 24 h of incubation, the culture supernatants were collected and analyzed for cytokine production. The concentrations of IL-12 p40 and IFN-α in culture supernatants were determined by enzyme-linked immunosorbent assays (ELISAs). ELISA kits for OptEIA mouse IL-12 p40 Set and mouse IFN-α were purchased from BD PharMingen (San Diego, Calif.) and PBL Biomedical Laboratories (New Brunswick, N.J.), respectively. Total RNAs were isolated by the use of Sepazol-RNA I (Nacalai Tesque, Kyoto, Japan), electrophoresed, and transferred to nylon membranes. Hybridization was performed with the indicated cDNA probes as previously described (2). cDNA probes specific for IL-12 p40 were established as previously described (31). To determine the effects of infection with AcNPV on cytokine production, we seeded the mouse macrophage cell line RAW264.7 into six-well plates at a concentration of 10^6 cells/well and stimulated them with various TLR ligands, with or without endosomal inhibitors such as chloroquine, bafilomycin A1, MDC, and ammonium chloride. For cell stimulation, AcNPV (5 μg/ml), LPS (10 ng/ml), PGN (2.5 μg/ml), and mCpG (200 ng/ml) were used.

Preparation of splenic dendritic cells and cytokine secretion. To prepare splenocytes containing dendritic cells (DCs), we cut spleen tissues into small fragments and incubated them with RPMI 1640 containing 400 U of collagenase (Wako)/ml and 15 μg of DNase (Sigma-Aldrich)/ml at 37°C for 20 min. For the last 5 min, 5 mM EDTA was added, and single-cell suspensions were prepared after red blood cell lysis. $CD11c^+$ cells were purified by magnetic cell sorting with anti-CD11c microbeads (Miltenyi Biotec GmbH, Bergisch Gladbach, Germany) according to the manufacturer's instructions and were used as splenic DCs. Enriched cells containing >90% $CD11c^+$ cells were seeded into 96-well plates at a concentration of 10^5 cells/well and stimulated with various doses of AcNPV or loxoribine. Culture supernatants were collected, and the production of IL-12 p40 and IFN-α was determined by ELISAs.

Indirect immunofluorescence assay and flow cytometric analysis. 293T cells transfected with a plasmid encoding human TLR9 were dislodged with PBS containing 5 mM EDTA 48 h after transfection. The cells were incubated with PBS containing 2% FCS and an anti-Flag (M2) monoclonal antibody (1:1,000) (Santa Cruz Biotechnology) for 1 h at 4°C, washed twice with PBS containing 2% FCS, and further incubated with fluorescein isothiocyanate-conjugated goat anti-mouse immunoglobulin G (IgG) (Sigma-Aldrich) in PBS containing 2% FCS for 1 h at 4°C. The cells were then fixed with 4% paraformaldehyde for 20 min, and the surface expression of human TLR9 was observed by fluorescence microscopy (UFX-II microscope; Nikon, Tokyo, Japan). Intracellular staining was examined after permeabilization with 0.5% Triton X-100. Stained cells were also analyzed by flow cytometry with a FACSCalibur instrument (Becton Dickinson, San Jose, Calif.), and the data were analyzed with CellQuest software (Becton Dickinson).

NF-κB–luciferase reporter gene assays with 293T cells. 293T cells were transfected with an NF-κB-dependent luciferase reporter plasmid (pELAM-Luc) together with human TLR9 expression vectors by the use of Lipofectamine 2000 (Life Technologies, Grand Island, N.Y.). pELAM-Luc (kindly provided by D. T. Golenbock) contains a human E-selectin promoter introduced into the pGL3 reporter plasmid (Promega, Inc., Madison, Wis.). The human TLR9 expression vector (kindly provided by T. H. Chuang) consists of a preprotrypsin signal peptide and a Flag epitope tag followed by an in-frame human TLR9 cDNA sequence (14). At 24 h posttransfection, the cells were stimulated with hCpG DNA (10 μg/ml) or AcNPV DNA (10 μg/ml) for 24 h. The luciferase activity was determined as previously described (49) and calculated as the degree of induction compared with an untreated control.

Detection of AcNPV capsid protein in murine macrophage cells by Western blot analysis. RAW264.7 murine macrophage cells (10^6 cells/well) infected with AcNPV at a dose of 40 μg/ml were washed extensively after 1 h of adsorption and harvested after 4 or 6 h of incubation. The cells were lysed in buffer containing 1% Triton X-100, 135 mM NaCl, 20 mM Tris-HCl (pH 7.5), 1% glycerol, and protease inhibitor cocktail tablets (Roche Molecular Biochemicals, Mannheim, Germany). The lysed sample was separated by SDS–12.5% PAGE and transferred to polyvinylidene difluoride membranes (Millipore, Tokyo, Japan). An anti-p39 mouse monoclonal antibody was used to detect the AcNPV capsid protein, which was visualized with the SuperSignal West Femto chemiluminescent substrate (Pierce).

RESULTS

Immune system activation by AcNPV is not mediated by viral envelope glycoprotein. It was previously reported that an IFN-stimulating preparation purified from Sf-9 cells infected with AcNPV exhibited IFN production both in vitro and in vivo

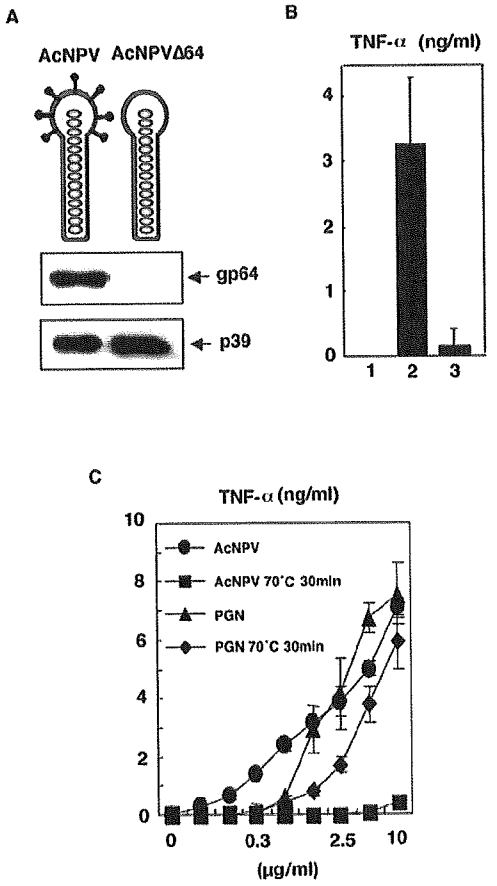

FIG. 1. Immune system activation of macrophages by heat-denatured or gp64-deficient AcNPV. (A) Purified particles of the mutant virus, AcNPVΔ64, lack gp64, as assayed by immunoblotting. (B) The production of TNF-α in RAW264.7 cells (10^6 cells/well) inoculated with AcNPV (5 μg/ml) (bar 2) or AcNPVΔ64 (5 μg/ml) (bar 3) was determined 24 h after inoculation by a sandwich ELISA. 1 is an uninfected control. Data are shown as means ± SD. (C) AcNPV and PGN were incubated at 70°C for 30 min. Treated and untreated samples were inoculated into RAW264.7 cells (10^6 cells/well) and incubated for 24 h. The production of TNF-α was determined by a sandwich ELISA. Data are shown as means ± SD.

and that induction was inhibited by monoclonal antibodies against the AcNPV envelope glycoprotein gp64 (18). To verify these observations, we constructed a mutant baculovirus lacking gp64, which we called AcNPVΔ64, and examined its ability to stimulate an immune response in RAW264.7 cells, which are highly sensitive to TLR stimulation and respond by producing inflammatory cytokines at a level comparable to that observed in primary macrophages (1). The absence of gp64 in purified particles of AcNPVΔ64 was confirmed by immunoblotting (Fig. 1A). The mutant virus lost the ability to induce TNF-α production in inoculated RAW264.7 cells (Fig. 1B), a result that is consistent with the previous observation that gp64 appears to play an important role in the induction of the immune response by AcNPV (18). Because some microbial products are known to induce cytokine production in macrophages, it was important to eliminate the possibility that contamination with microbial products contributed to the immune system

activation by AcNPV. Although the stimulation of macrophages by AcNPV was completely eliminated by incubation at 70°C for 30 min (Fig. 1C), stimulation by the bacterial components PGN and LPS was resistant to heat treatment (Fig. 1C and data not shown). These data indicate that the activation of macrophages by AcNPV is mediated by heat-labile viral components rather than by LPS and PGN.

To further verify the involvement of gp64 in immune system stimulation by baculovirus, we prepared expression plasmids encoding both wild-type gp64 and a C-terminally truncated gp64 protein (gp64ΔTM) with a C-terminal His_6 tag to allow for purification. Upon transfection of Sf9 cells, both recombinant proteins were detected, while gp64ΔTM was efficiently secreted into the culture supernatant (Fig. 2A). The protein from cells expressing gp64ΔTM was purified by column chromatography, producing a single band corresponding to gp64ΔTM and comparable to viral gp64 (Fig. 2B). We also tried to obtain the wild-type gp64 protein from the cell lysates but could not purify it to a homogeneous band (data not shown).

The activities of AcNPV, gp64ΔTM, and PGN on RAW264.7 cells were then examined. A dose-dependent induction of TNF-α and IL-6 was observed for RAW264.7 cells treated with AcNPV and PGN, whereas cytokine production was not observed for cells treated with gp64ΔTM (Fig. 2C). In addition, gp64ΔTM was not able to induce IFN-α production in RAW264.7 cells (Fig. 2D). Furthermore, the pretreatment of macrophage cells with gp64ΔTM inhibited immune system activation by AcNPV but had no effect on the activation by PGN (Fig. 2E), suggesting that the gp64ΔTM protein still retained some of the biological functions of the wild-type gp64 protein, at least in terms of its interaction with host cells. These results indicated that gp64 is an essential element of AcNPV-induced immune system activation in RAW264.7 cells but that it does not directly participate in the reaction. Viral components other than gp64 may be more directly involved in this process.

AcNPV induces inflammatory cytokine production through a MyD88/TLR9-dependent pathway. Immune cells from MyD88- or TLR-deficient mice are unresponsive to TLR ligands, as assayed by their levels of cytokine production (5). Therefore, we used PECs and splenic $CD11c^+$ DCs obtained from MyD88- and TLR-deficient mice to determine whether or not the TLR signaling pathway is responsible for the activation by AcNPV. Thioglycolate-elicited PECs were isolated from wild-type, $MyD88^{-/-}$, $TLR2^{-/-}$, $TLR4^{-/-}$, and $TLR9^{-/-}$ mice and examined by ELISA and Northern blot analysis for the induction of IL-12 following exposure to AcNPV. Wild-type macrophages inoculated with AcNPV produced large amounts of IL-12 in a dose-dependent manner, whereas MyD88- or TLR9-deficient macrophages had severely reduced IL-12 production (Fig. 3A). PECs from $TLR2^{-/-}$ and $TLR4^{-/-}$ mice produced IL-12 at wild-type levels in response to AcNPV (Fig. 3A).

Loxoribine is a potent inducer of cytokine production in macrophages and functions through a TLR7-dependent pathway (36). PECs from wild-type, $TLR2^{-/-}$, $TLR4^{-/-}$, and $TLR9^{-/-}$ mice all produced IL-12 in response to loxoribine, whereas no IL-12 production was observed in PECs from $MyD88^{-/-}$ mice (Fig. 3A). The transcription of IL-12 p40 mRNA was also impaired in MyD88- and TLR9-deficient macrophages stimulated with AcNPV (Fig. 3B). We further examined the response of splenic $CD11c^+$ DCs to AcNPV and loxoribine. Wild-type and $TLR4^{-/-}$ splenic $CD11c^+$ DCs produced IL-12 in response to AcNPV in a dose-dependent manner, whereas the production of IL-12 was severely impaired in $MyD88^{-/-}$ and $TLR9^{-/-}$ mice (Fig. 3C). In response to loxoribine, splenic $CD11c^+$ DCs from $TLR4^{-/-}$ and $TLR9^{-/-}$ mice exhibited higher IL-12 production levels than wild-type cells, whereas the production of IL-12 was completely inhibited in $MyD88^{-/-}$ mice (Fig. 3C). These results indicate that AcNPV induces the production of inflammatory cytokines in immunocompetent cells through a MyD88/TLR9-dependent pathway.

AcNPV produces IFN-α through a MyD88/TLR9-independent pathway. IFNs are important mediators of the early host defense against various viral infections. Since AcNPV has also been shown to be a potent inducer of IFN-α (Fig. 2D) (18), we investigated whether IFN-α production induced by AcNPV is dependent on the MyD88 and TLR9 signaling pathways. Although IFN-α induction by the TLR9 ligand, CpG oligonucleotides, was completely abolished in PECs and splenic $CD11c^+$ DCs derived from $MyD88^{-/-}$ or $TLR9^{-/-}$ mice (data not shown), IFN-α production in response to AcNPV was less impaired (Fig. 4A). This contrasted sharply with the complete loss of IL-12 production observed for these cells (Fig. 3). Macrophages from $MyD88^{-/-}$ and $TLR9^{-/-}$ mice exhibited a slight reduction in IFN-α and IFN-β mRNA transcription in response to AcNPV (Fig. 4B). These results indicate that AcNPV induces the production of inflammatory cytokines in immunocompetent cells through a MyD88/TLR9-dependent pathway, while other MyD88/TLR9-independent pathways are also involved in the production of IFNs.

AcNPV DNA stimulates immune system activation in macrophage cell lines. CpG motifs present in the genomes of many bacteria are unmethylated, whereas eukaryotic genomes are much more likely to undergo methylation. Previous work demonstrated that bacterial DNAs and certain oligonucleotides containing unmethylated CpG dinucleotides can stimulate PECs and DCs (19, 32). In addition, TLR9 is essential for the immune response to CpG-rich DNA, since TLR9-deficient mice are refractory to such stimulation (24). The frequency of bioactive CpG motifs in the AcNPV genome was similar to that observed for *Escherichia coli* and HSV DNAs (61) and significantly higher than that in murine and entomopoxvirus DNAs (Table 1).

To determine the methylation status of the AcNPV genome, we digested DNAs isolated from AcNPV, Sf-9 cells, *E. coli*, and 293T cells with the restriction enzyme HpaII, which cannot cleave when the cytosine adjacent to the cleavage site (CC ↓ GG) is methylated. While DNA isolated from 293T cells was refractory to HpaII digestion, DNAs from AcNPV, Sf-9 cells, and *E. coli* were sensitive to HpaII digestion, indicating that most of the CpG dinucleotides in AcNPV were unmethylated (Fig. 5A).

To determine the ability of AcNPV DNA to stimulate an immune response in vitro, we purified the viral DNA from virions. RAW264.7 cells were then treated with purified viral DNA or PGN with or without liposomes (Fig. 5B). The transfection of viral DNA with liposomes resulted in the production

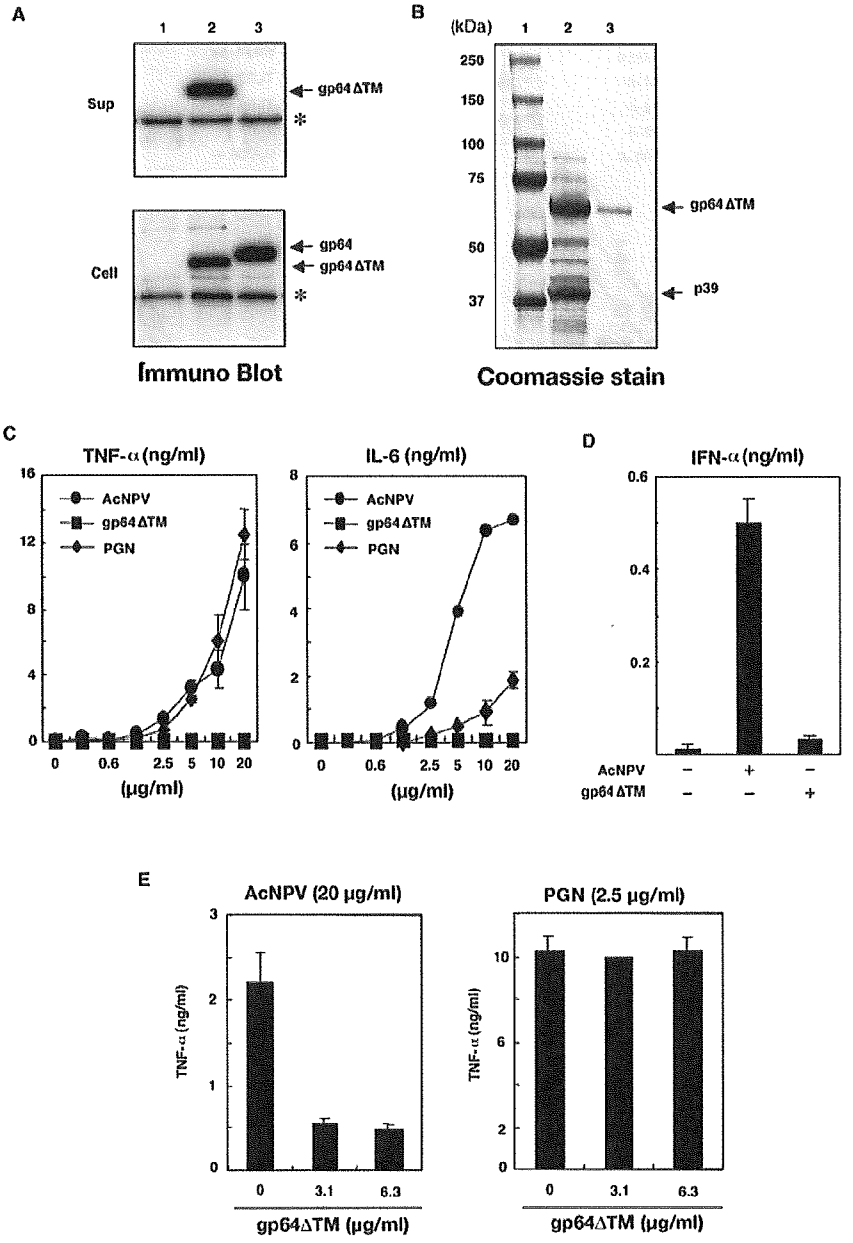

FIG. 2. Immune system activation by AcNPV in macrophages is not mediated by gp64. (A) Wild-type gp64 and a deletion mutant lacking the transmembrane region of the gp64 envelope protein (gp64ΔTM) were expressed in Sf-9 cells. Whole-cell lysates and culture supernatants were subjected to SDS-PAGE under reducing conditions and visualized by immunoblotting with an antihexahistidine monoclonal antibody. Lane 1, cells transfected with pIB/V5-His; lanes 2 and 3, cells transfected with pIBgp64ΔTM/V5-His and pIBgp64/V5-His, respectively. The heavy chains of the antibody are indicated by asterisks. (B) Purified AcNPV virions (lane 2) and gp64ΔTM (lane 3) were analyzed by SDS-PAGE and Coomassie blue staining. Lane 1, molecular mass markers. (C) Activation of mouse macrophage RAW264.7 cells (10^6 cells/well) treated with the indicated amounts of AcNPV or gp64ΔTM. The production of TNF-α and IL-6 in culture supernatants after 24 h of incubation was determined by sandwich ELISAs. PGN was used as a positive control. Data are shown as means ± SD. (D) Production of IFN-α in RAW264.7 cells (10^6 cells/well) inoculated with AcNPV (5 μg/ml) or gp64ΔTM (5 μg/ml), as determined by a sandwich ELISA after 24 h of incubation. Data are shown as means ± SD. (E) Production of TNF-α in RAW264.7 cells (10^6 cells/well) inoculated with AcNPV (20 μg/ml) or PGN (2.5 μg/ml), with or without a pretreatment with the indicated amounts of gp64ΔTM for 2 h at 37°C. After 24 h of incubation, the production of TNF-α in culture supernatants was determined by a sandwich ELISA. Data are shown as means ± SD.

of TNF-α, but this effect was not observed in the absence of liposomes. The enhancement of TNF-α production by liposomes was not observed in cells treated with PGN, and the addition of liposomes alone did not elicit TNF-α production (Fig. 5C). These results indicate that the internalization of viral DNA is necessary for the activation of the AcNPV-mediated TLR9 signaling pathway. Thus, the impaired immune system activation by AcNPVΔ64 in macrophages may result from a

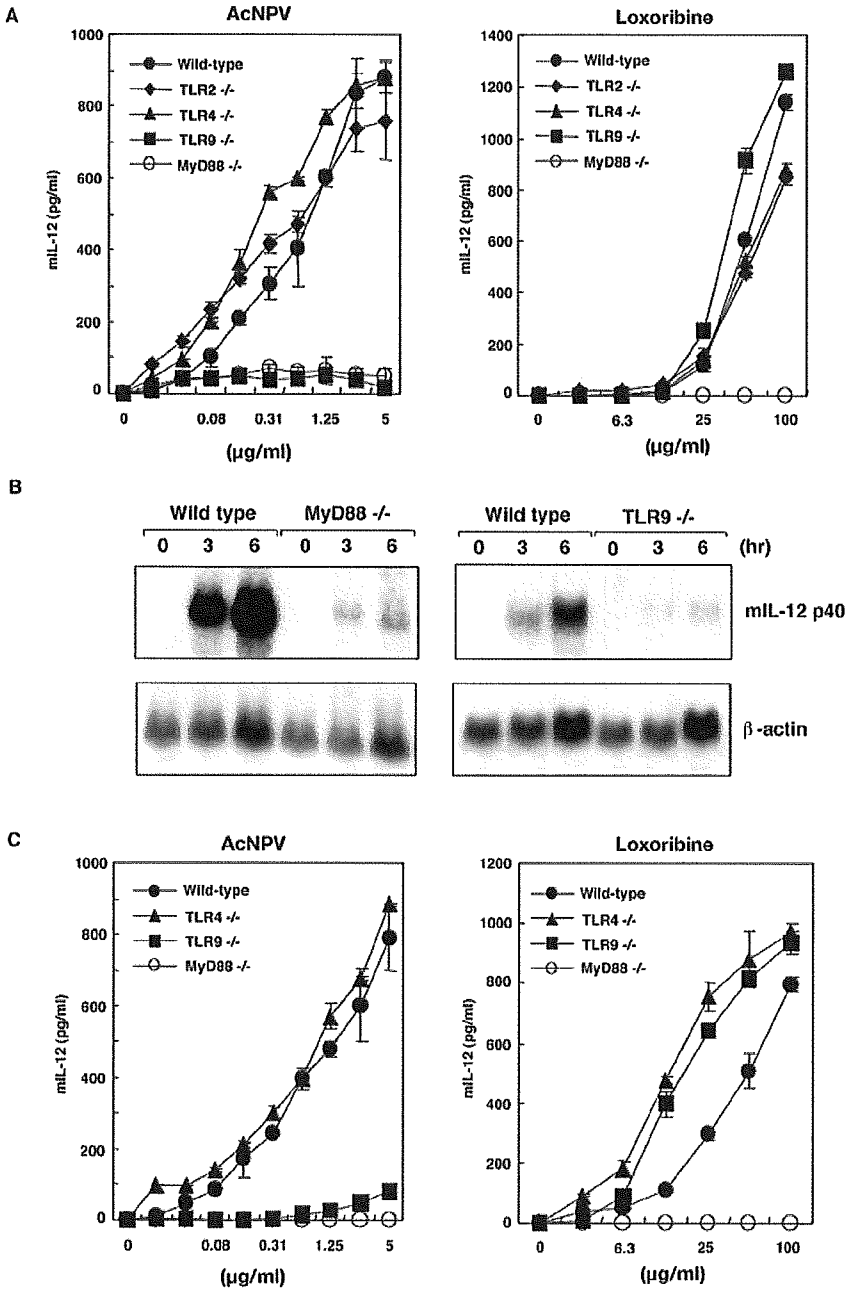

FIG. 3. AcNPV activates PECs and DCs in a MyD88/TLR9-dependent manner. (A) PECs (2×10^5 cells/well) from wild-type (C57BL/6) or MyD88-, TLR2-, TLR4-, or TLR9-deficient mice were stimulated with the indicated amounts of AcNPV or loxoribine. The production of IL-12 p40 in culture supernatants was measured by a sandwich ELISA. Data are shown as means ± SD. (B) Northern blot analysis of murine macrophage cells stimulated with AcNPV. PECs (6×10^6 cells/well) from wild-type or MyD88- or TLR9-deficient mice were stimulated with AcNPV (10 μg/ml) for the indicated times. Total RNAs were extracted and subjected to Northern blot analysis. (C) Splenic $CD11c^+$ DCs were prepared from wild-type or MyD88-, TLR4-, or TLR9-deficient mice and enriched by magnetic cell sorting. Splenic DCs (10^5 cells/well) were stimulated with the indicated amounts of AcNPV or loxoribine for 24 h. The production of IL-12 p40 in supernatants was measured by a sandwich ELISA. Data are shown as means ± SD.

failure to internalize viral DNA via gp64-mediated membrane fusion.

To further confirm that viral DNA activates the signaling pathway following internalization via gp64, we inactivated AcNPV by UV irradiation and examined the production of TNF-α in RAW264.7 cells. UV irradiation diminished the AcNPV-mediated induction of TNF-α, but the addition of liposomes restored the activation (Fig. 5C). These results

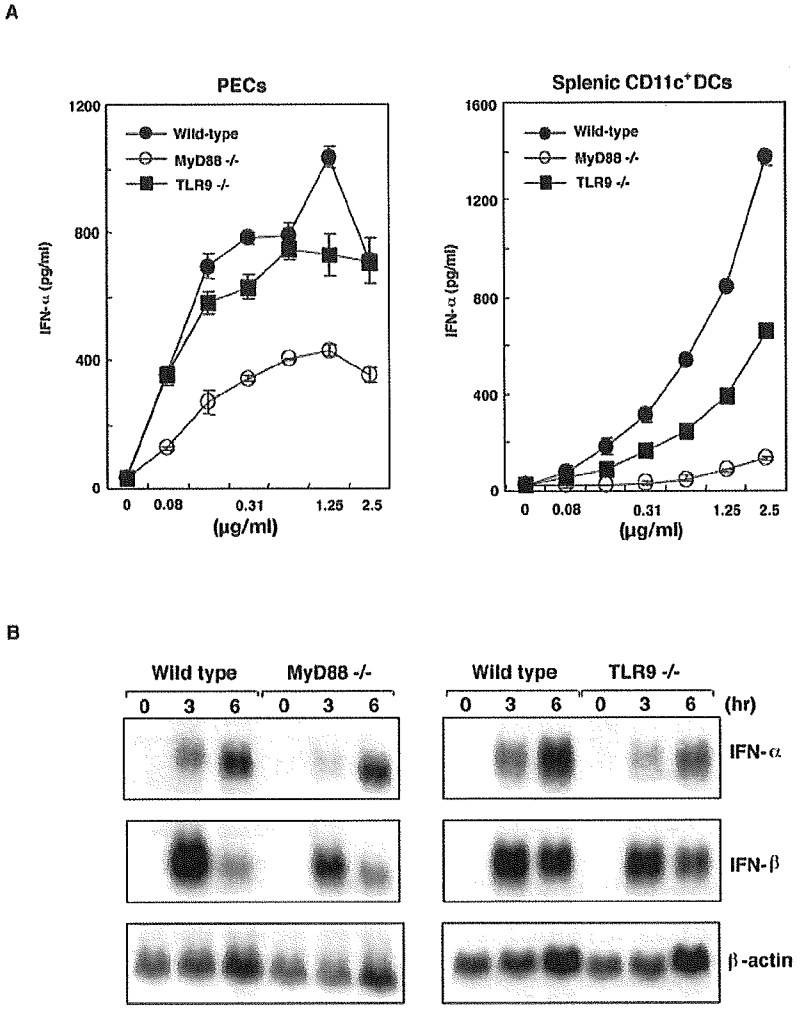

FIG. 4. IFN production by AcNPV is mediated by a MyD88/TLR9-independent process. (A) PECs (2×10^5 cells/well) and splenic CD11c$^+$ DCs (1×10^5 cells/well) were prepared from wild-type or MyD88- or TLR9-deficient mice and stimulated with the indicated amounts of AcNPV or loxoribine for 24 h. The production of IFN-α in culture supernatants was measured by a sandwich ELISA. Data are shown as means ± SD. (B) Northern blot analysis of murine macrophage cells stimulated with AcNPV. PECs (6×10^6 cells/well) from wild-type or MyD88- or TLR9-deficient mice were stimulated with AcNPV (10 μg/ml) for the indicated times. Total RNAs were then extracted and subjected to Northern blot analysis.

suggest that the denaturation of gp64 by UV irradiation impaired the fusion capability of the envelope protein, thus inhibiting the internalization of viral DNA into the cell via membrane fusion.

AcNPV DNA induces NF-κB activation through human TLR9. Signaling via TLRs occurs through the sequential recruitment of the adapter molecule MyD88 and the serine-threonine kinase IL-1 receptor-associated kinase, which leads to the activation of mitogen-activated protein kinases and the nuclear factor NF-κB (51). To assess whether or not the expression of human TLR9 confers cellular responsiveness to AcNPV DNA, we transfected 293T cells with a human TLR9 expression plasmid and a pELAM luciferase reporter plasmid together with AcNPV or hCpG, which was used as a positive control (Fig. 6A). Although NF-κB activation was not observed for cells transfected with undigested AcNPV DNA,

TABLE 1. CpG motif frequencies in AcNPV and other genomes[a]

Motif	Frequency of appearance				
	E. coli	Mouse	HSV-1	AcNPV	AmEPV
CACGTT	1.30	0.11	0.76	0.90	0.17
AGCGTT	1.70	0.17	0.42	1.12	0.15
AACGTC	0.60	0.11	0.73	0.98	0.17
AGCGTC	1.30	0.15	0.85	0.85	0.15
GGCGTC	1.40	0.15	4.0	1.10	0.02
GGCGTT	2.50	0.15	1.51	1.37	0.10
Average	1.53	0.14	1.38	1.05	0.13

[a] The frequency at which each CpG hexamer appeared in the *E. coli*, mouse, HSV-1, AcNPV, and *Amsacta moorei* entomopoxvirus genomes was determined by using published sequence data. The GenBank accession numbers for the complete genomes of AcNPV and AmEPV are NC 001623 and NC 002520, respectively. The complete genomes of *E. coli* K-12 and HSV-1 and mouse chromosome sequences were described previously (61).

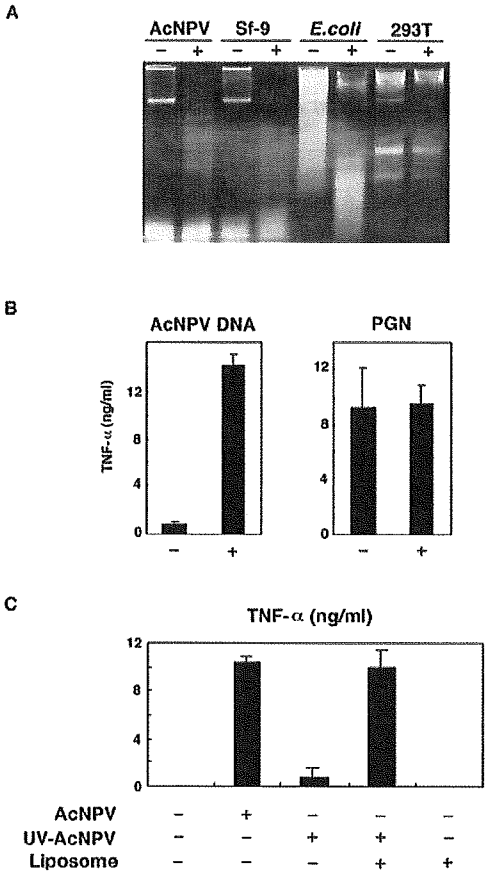

FIG. 5. Activation of mouse macrophage cell line by AcNPV DNA. (A) Methylation status of genomic DNA. Genomic DNAs obtained from AcNPV, Sf-9 cells, *E. coli*, and 293T cells were digested with the methylation-sensitive restriction enzyme HpaII. Undigested (−) and digested (+) samples were analyzed by agarose gel electrophoresis. (B) RAW264.7 cells (10^6 cells/well) were treated with AcNPV DNA (5 μg/ml) or PGN (2.5 μg/ml) in the absence (−) or presence (+) of liposomes for 24 h, and the production of TNF-α in culture supernatants was determined by a sandwich ELISA. Data are shown as means ± SD. (C) Activation of RAW264.7 cells (10^6 cells/well) inoculated with untreated or UV-inactivated AcNPV (5 μg/ml) in the presence or absence of liposomes was assessed by the production of TNF-α in culture supernatants. Data are shown as means ± SD.

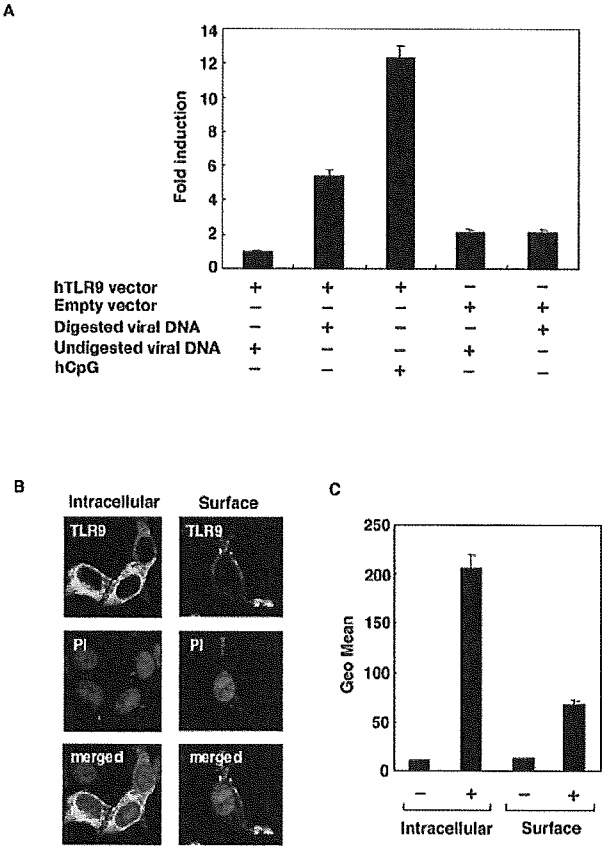

FIG. 6. AcNPV DNA induces NF-κB activation through human TLR9. (A) 293T cells were transfected with an empty or human TLR9 expression vector together with a pELAM luciferase reporter plasmid. Twenty-four hours after transfection, the cells were stimulated with digested or undigested AcNPV DNA (10 μg/ml). hCpG (10 μg/ml) was used as a positive control. The luciferase activity was determined at 24 h posttransfection and expressed as the level of induction compared with that detected in cells transfected with the human TLR9 expression vector alone. Data are shown as means ± SD. (B) Immunofluorescence micrographs of 293T cells transfected with an N-terminal Flag-tagged human TLR9 expression vector and stained with an anti-Flag (M2) monoclonal antibody. The intracellular (left) and cell surface (right) expression of TLR9 is shown. Nuclei were stained with propidium iodide (PI). Samples were observed by confocal microscopy. (C) The surface and intracellular expression of human TLR9 in 293T cells transfected with an N-terminal Flag-tagged human TLR9 expression vector (+) or an empty vector (−) and stained with an anti-Flag monoclonal antibody was examined by fluorescence-activated cell sorting.

HindIII-digested viral DNA and hCpG exhibited significant NF-κB activation, suggesting that undigested viral DNA is incapable of penetrating cells by transfection. No activation of NF-κB was observed in 293T cells cotransfected with a human TLR2 or TLR4 expression plasmid when stimulated with digested AcNPV DNA (data not shown).

Recent work demonstrated that the endogenous expression of TLR3, TLR7, TLR8, and TLR9 was mainly detected in the cytoplasmic vesicles of macrophages (58). To examine the localization of transiently expressed TLR9, we transfected 293T cells with a TLR9 expression plasmid and examined TLR9 expression by immunofluorescence microscopy and cell sorting. The expression of TLR9 in the cytoplasm was three times higher than that at the cell surface (Fig. 6B and C). These results indicate that the introduction of AcNPV DNA into the cytoplasm is specifically detected by human TLR9 and results in the activation of NF-κB.

AcNPV requires endosomal maturation to induce immune system activation in macrophages. To further explore the role of endocytosis in the signal transduction pathway triggered by AcNPV DNA, we examined the effect of endosomal maturation or acidification inhibitors. As shown in Fig. 7A, chloroquine was able to inhibit immune system activation of RAW264.7 cells treated with AcNPV and mCpG oligonucleotides in a dose-dependent manner, but no inhibition of LPS or PGN activation was observed. Other inhibitors of endoso-

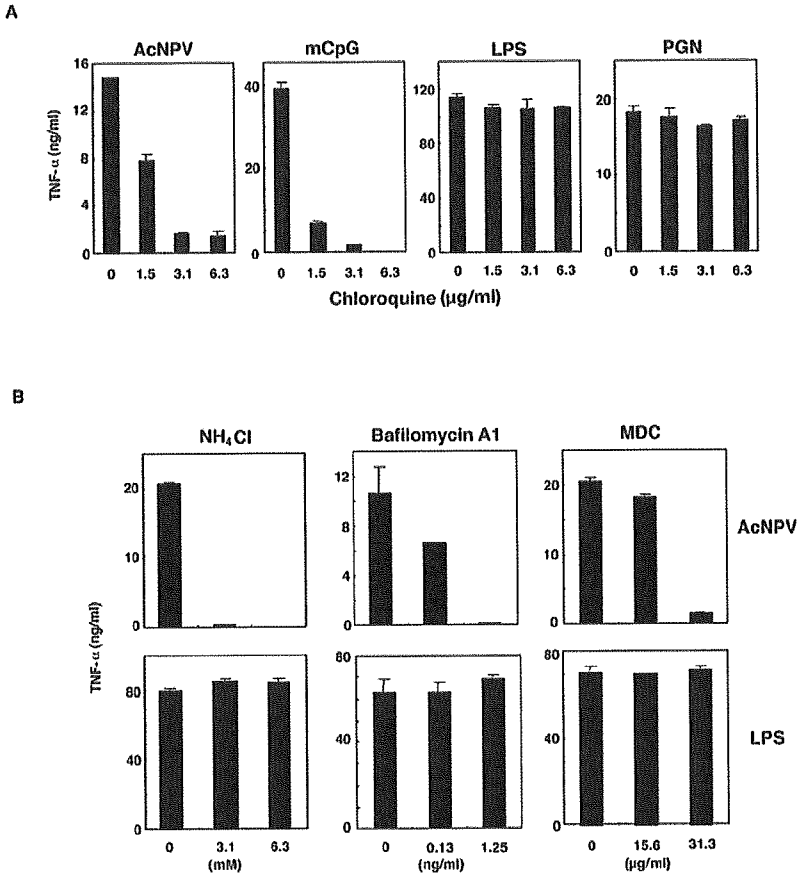

FIG. 7. AcNPV requires endosomal maturation to induce immune system activation in macrophages. (A) RAW264.7 cells (10^6 cells/well) were stimulated with AcNPV (5 μg/ml), mCpG (200 ng/ml), LPS (10 ng/ml), or PGN (2.5 μg/ml) at the indicated concentrations of chloroquine. After 24 h of incubation, the production of TNF-α in culture supernatants was determined by a sandwich ELISA. Chloroquine was added to the cells 2 h before stimulation. Data are shown as means ± SD. (B) RAW264.7 cells (10^6 cells/well) were treated with AcNPV (5 μg/ml) or LPS (10 ng/ml) and with the indicated concentrations of endosomal maturation inhibitors. After 24 h of incubation, the production of TNF-α in culture supernatants was determined by a sandwich ELISA. The inhibitors were added to the cells 2 h before stimulation. Data are shown as means ± SD.

mal maturation, such as ammonium chloride, bafilomycin A1, and MDC, inhibited AcNPV-induced, but not LPS-induced, immune system activation (Fig. 7B). Together with our other data, these results indicate that endosomal acidification and/or maturation is a key step in AcNPV-induced immune system activation via TLR9, a process that requires the release of the viral genome into TLR9-expressing cytoplasmic vesicles following the internalization of viral DNA by endocytosis through gp64-mediated membrane fusion.

AcNPV penetrates macrophages via the phagocytic pathway. To further confirm that baculovirus was internalized into macrophages, we inoculated RAW264.7 cells with a recombinant baculovirus carrying a luciferase gene under the control of a mammalian promoter, AcCAGluc (49). As shown in Fig. 8A, the expression of luciferase was observed in 293T cells, but not RAW264.7 cells, that were infected with AcCAGluc. The viral capsid protein was clearly detected by immunoblotting for both 293T and RAW264.7 cells infected with AcNPV, but the protein level was greatly diminished in RAW264.7 cells by 6 h postinoculation, probably as a result of degradation (Fig. 8B). These results suggest that baculovirus can penetrate into different cells via gp64-mediated endocytosis but that it translocates into different subcellular compartments in different cells. In 293T cells, the nucleocapsid was apparently able to reach the nucleus, where the reporter gene was efficiently transcribed following uncoating. However, in the immunocompetent RAW264.7 cells, the nucleocapsid appeared to have been trapped by the phagocytic pathway, and degraded viral DNA was then translocated into TLR9-expressing intracellular compartments (58).

DISCUSSION

We have previously demonstrated that intranasal inoculation with AcNPV induces a strong innate immune response that protects mice from a lethal challenge with influenza virus (1). The lungs of mice inoculated with AcNPV exhibited a marked infiltration of macrophages, which presumably inhibit the growth of influenza virus in the lung tissues. The baculovirus envelope glycoprotein gp64 contains mannose, fucose,

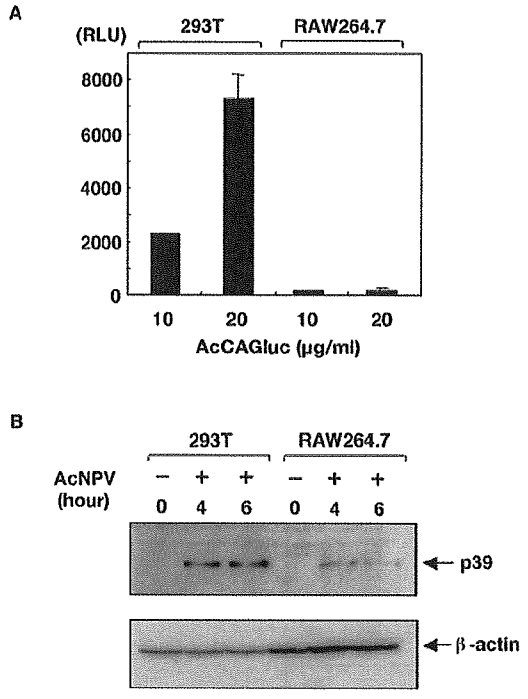

FIG. 8. AcNPV penetrates macrophages through the phagocytic pathway. (A) 293T and RAW264.7 cells (10^6 cells/well) were inoculated with a recombinant baculovirus possessing the luciferase gene under the control of the CAG promoter, AcCAGluc (49) (10 and 20 μg/ml). Cells were harvested 24 h after infection, and relative luciferase activities were determined. (B) 293T and RAW264.7 cells (10^6 cells/well) were inoculated with AcCAGluc (40 μg/ml), washed extensively after 1 h of adsorption, and harvested after 4 or 6 h of incubation. The presence of the p39 capsid protein in cells inoculated with AcNPV was determined by immunoblotting with an anti-p39 monoclonal antibody.

and *N*-acetyl-glucosamine modifications but no detectable galactose or terminal sialic acid residues (29). The mannose receptor (MR) recognizes a range of carbohydrates present on the surfaces and cell walls of microorganisms. MR is primarily expressed on macrophages and DCs and is involved in MR-mediated endocytosis and phagocytosis. In addition, MR plays a key role in host defense and the induction of innate immunity (8). Therefore, it is tempting to speculate that gp64 interacts with MR through its mannose modifications in macrophages and DCs of mice inoculated with AcNPV. However, our data contradict such a model; instead, we show that it is AcNPV DNA, not the gp64 glycoprotein, that induces immune system activation in a MyD88/TLR9-dependent manner.

Recently, it was shown that plasmacytoid DCs (pDCs) naturally produce IFN-α in response to viruses (30). HSV-1 and -2, whose genomes contain abundant CpG motifs, are able to induce the production of IFN-α in pDCs. The HSV-induced production of IFN-α in pDCs derived from MyD88- and TLR9-deficient mice was completely eliminated (33, 40). The recognition of the HSV genome by TLR9 was shown to be mediated by an endocytic pathway that can be inhibited by chloroquine or bafilomycin A1. In this study, we demonstrated that AcNPV induces proinflammatory cytokines through a MyD88/TLR9-dependent signaling pathway, whereas signaling molecules other than MyD88 may participate in IFN-α production in response to AcNPV. Recently, MyD88-independent TLR signaling events involving TIR domain-containing adaptor inducing IFN-β (TRIF) were described (59). Therefore, it is possible that the TRIF pathway is one means by which AcNPV induces MyD88-independent IFN production. However, future studies are needed to clarify the precise mechanisms of this induction.

While UV irradiation of AcNPV abolishes its ability to stimulate an immune response, the addition of liposomes is able to restore this activity. UV-inactivated HSV is capable of inducing the production of IFN-α in pDCs (40), indicating that viral replication is not required for the HSV-induced immune response. In contrast, UV irradiation of AcNPV abolishes immune stimulation in macrophages, while internalization of the inactivated virus by liposomes restores the activity. These results, in conjunction with our data for AcNPVΔ64, indicate that the AcNPV-induced production of cytokines in immunocompetent cells requires a fusion process mediated by gp64 that leads to internalization of the viral genome into the cells.

Recently, several viral envelope glycoproteins were shown to induce immune system activation through TLRs (10, 22, 34, 47). However, gp64 does not directly participate in a TLR-mediated immune response. TLR family members are expressed differentially at very low levels on the surfaces of different immune cells and appear to respond to different stimuli (43). A recent study indicated that LPS and CpG-rich DNA activate TLRs in distinct cellular compartments (3). Internalization and endosomal maturation are required for CpG-rich DNA to activate TLR9, but not for LPS to activate TLR4 on the plasma membrane. We showed here that the inhibition of endosomal maturation by a treatment with chloroquine abolishes the immune system activation of AcNPV in a dose-dependent manner. These results imply that immune system activation by AcNPV through TLR9 requires membrane fusion via gp64 as well as the liberation of the viral genome into cytoplasmic vesicles expressing TLR9.

Interestingly, Lund et al. demonstrated that the TLR7-mediated immune recognition of single-stranded RNAs from vesicular stomatitis virus and influenza virus requires endosomal acidification (41). The recognition of HSV-1 and HSV-2 viral DNAs through a TLR9/MyD88-dependent pathway in pDCs also requires endosomal acidification (40). These data indicate that TLR7 and TLR9 expressed in the endosomal or lysosomal compartments of immunocompetent cells recognize the viral genome entering the cell through receptor-mediated endocytosis or phagocytosis, leading to the secretion of inflammatory cytokines and IFNs. However, the precise mechanisms by which viral genomes translocate to TLR-expressing compartments are still unknown.

Since the first report on the immunostimulatory potential of bacterial DNA, which found that the main immunogenic fraction of mycobacterial lysates consists of genomic DNA (55, 56), substantial progress has been made towards understanding the immunostimulatory potency of CpG-rich DNA motifs, which are more common in bacteria than in vertebrates. For instance, TLR9 was shown to be responsible in vivo for immune system stimulation by oligodeoxynucleotides containing unmethylated CpG motifs (24). Like bacteria, AcNPV contains a significant

number of potentially bioactive CpG motifs. Interestingly, the frequency of CpG motifs in HSV DNA, which has been shown to be involved in the induction of angiogenesis in stromal keratitis (61), was similar to that in *E. coli* DNA. In contrast, the frequency of CpG motifs in the genome of an insect poxvirus was much lower than that for AcNPV (Table 1).

In conclusion, we have demonstrated that AcNPV has the ability to induce innate immune system activation through a MyD88/TLR9-dependent pathway. The molecular mechanisms of viral uptake, intracellular processing, and the induction of potent antiviral activity in immune cells require further investigation. However, the strong immune response induced by AcNPV makes it a promising candidate for a novel, adjuvant-containing vaccine vehicle against infectious diseases. In particular, our findings raise the possibility that AcNPV may be harnessed therapeutically to induce a host immune response against various infectious diseases caused by pathogens invading the respiratory tract.

ACKNOWLEDGMENTS

We are grateful to T. H. Chuang for providing us with the TLR9 expression plasmid, D. T. Golenbock for the pELAM Luc plasmid, and G. F. Rohrmann for the p39 monoclonal antibody. We also thank I. Yanase and H. Murase for secretarial work. T.A. and H.H. are Research Fellows of the Japan Society for the Promotion of Science.

This work was supported by grants-in-aid from the Ministry of Health, Labor and Welfare in Japan to Y.M. and from the 21st Century Center of Excellence Program of Japan to Y.M. and S.A.

REFERENCES

1. **Abe, T., H. Takahashi, H. Hamazaki, N. Miyano-Kurosaki, Y. Matsuura, and H. Takaku.** 2003. Baculovirus induces an innate immune response and confers protection from lethal influenza virus infection in mice. J. Immunol. **171**:1133–1139.
2. **Adachi, O., T. Kawai, K. Takeda, M. Matsumoto, H. Tsutsui, M. Sakagami, K. Nakanishi, and S. Akira.** 1998. Targeted disruption of the MyD88 gene results in loss of IL-1- and IL-18-mediated function. Immunity **9**:143–150.
3. **Ahmad-Nejad, P., H. Hacker, M. Rutz, S. Bauer, R. M. Vabulas, and H. Wagner.** 2002. Bacterial CpG-DNA and lipopolysaccharides activate Toll-like receptor at distinct cellular compartments. Eur. J. Immunol. **32**:1958–1968.
4. **Airenne, K. J., M. O. Hiltunen, M. P. Turunen, A. M. Turunen, O. H. Laitinen, M. S. Kulomaa, and S. Y. Herttuala.** 2000. Baculovirus-mediated periadventitial gene transfer to rabbit carotid artery. Gene Ther. **7**:1499–1504.
5. **Akira, S., K. Takeda, and T. Kaisho.** 2001. Toll-like receptors: critical proteins linking innate and acquired immunity. Nat. Immunol. **2**:675–680.
6. **Alexopoulou, L., A. C. Holt, R. Medzhitov, and R. A. Flavell.** 2001. Recognition of double-stranded RNA and activation of NF-κB by Toll-like receptor 3. Nature **413**:732–738.
7. **Aliprantis, A. O., R. B. Yang, M. R. Mark, S. Suggett, B. Devaux, J. D. Radolf, G. R. Klimpel, P. Godowski, and A. Zychlinsky.** 1999. Cell activation and apoptosis by bacterial lipoproteins through Toll-like receptor-2. Science **285**:736–739.
8. **Apostolopoulos, V., and I. F. McKenzie.** 2001. Role of the mannose receptor in the immune response. Curr. Mol. Med. **1**:469–474.
9. **Barsoum, J., R. Brown, M. Mckee, and F. M. Boyce.** 1997. Efficient transduction of mammalian cells by a recombinant baculovirus having the vesicular stomatitis virus G glycoprotein. Hum. Gene Ther. **8**:2011–2018.
10. **Bieback, K., E. Lien, I. M. Klagge, E. Avota, J. Schneider-Schaulies, W. P. Duprex, H. Wagner, C. J. Kirschning, V. Ter Meulen, and S. Schneider-Schaulies.** 2002. Hemagglutinin protein of wild-type measles virus activates Toll-like receptor 2 signaling. J. Virol. **76**:8729–8736.
11. **Bowie, A., E. Kiss-Toth, J. A. Symons, G. L. Smith, S. K Dower, and L. A. O. Neill.** 2000. A46R and A52R from vaccinia virus are antagonists of host IL-1 and Toll-like receptor signaling. Proc. Natl. Acad. Sci. USA **97**:10162–10167.
12. **Boyce, F. M., and N. L. R. Bucher.** 1996. Baculovirus mediated gene transfer into mammalian cells. Proc. Natl. Acad. Sci. USA **93**:2348–2352.
13. **Brightbill, H. D., D. H. Libraty, S. R. Krutzik, R. B. Yang, J. T. Belisle, J. R. Bleharski, M. Maitland, M. V. Norgard, S. E. Plevy, S. T. Smale, P. J. Brennan, B. R. Bloom, P. J. Godowski, and R. L. Modlin.** 1999. Host defense mechanisms triggered by microbial lipoproteins through Toll-like receptors. Science **285**:732–736.
14. **Chuang, T. H., J. Lee, L. Kline, J. C. Mathison, and R. J. Ulevitch.** 2002. Toll-like receptor 9 mediates CpG-DNA signaling. J. Leukoc. Biol. **71**:538–544.
15. **Compton, T., E. A. Kurt-Jones, K. W. Boehme, J. Belko, E. Latz, D. T. Golenbock, and R. W. Finberg.** 2003. Human cytomegalovirus activates inflammatory cytokine responses via CD14 and Toll-like receptor 2. J. Virol. **77**:4588–4596.
16. **Condreay, J. P., S. M. Witherspoon, W. C. Clay, and T. A. Kost.** 1999. Transient and stable gene expression in mammalian cells transduced with a recombinant baculovirus vector. Proc. Natl. Acad. Sci. USA **96**:127–132.
17. **Diebold, S. S., T. Kaisho, H. Hemmi, S. Akira, E. Reis, and C. Sousa.** 2004. Innate antiviral responses by means of TLR7-mediated recognition of single-stranded RNA. Science **303**:1529–1531.
18. **Gronowski, A. M., D. M. Hilbert, K. C. F. Sheehan, G. Garotta, and R. D. Schreiber.** 1999. Baculovirus stimulates antiviral effect in mammalian cells. J. Virol. **73**:9944–9951.
19. **Hacker, H., H. Mischak, T. Miethke, S. Liptay, R. Schmid, T. Sparwasser, K. Heeg, G. B. Lipford, and H. Wagner.** 1998. CpG-DNA-specific activation of antigen-presenting cells requires stress kinase activity and is preceded by non-specific endocytosis and endosomal maturation. EMBO J. **17**:6230–6240.
20. **Hacker, H., R. M. Vabulas, O. Takeuchi, K. Hoshino, S. Akira, and H. Wagner.** 2000. Immune cell activation by bacterial CpG-DNA through myeloid differential marker 88 and tumor necrosis factor receptor-associated factor (TRAF) 6. J. Exp. Med. **192**:595–600.
21. **Hayashi, F., K. D. Smith, A. Ozinsky, T. R. Hawn, E. C. Yi, D. R. Goodlett, J. K. Eng, S. Akira, D. M. Underhill, and A. Aderem.** 2001. The innate immune response to bacterial flagellin is mediated by Toll-like receptor 5. Nature **410**:1099–1103.
22. **Haynes, L. M., D. D. Moore, E. A. Kurt-Jones, R. W. Finberg, L. J. Anderson, and R. A. Tripp.** 2001. Involvement of Toll-like receptor 4 in innate immunity to respiratory syncytial virus. J. Virol. **75**:10730–10737.
23. **Heil, F., H. Hemmi, H. Hochrein, F. Ampenberger, C. Kirschning, S. Akira, G. Lipford, H. Wagner, and S. Bauer.** 2004. Species-specific recognition of single-stranded RNA via Toll-like receptor 7 and 8. Science **303**:1526–1529.
24. **Hemmi, H., O. Takeuchi, T. Kawai, T. Kaisho, S. Sato, H. Sanjo, M. Matsumoto, K. Hoshino, H. Wagner, K. Takeda, and S. Akira.** 2000. A Toll-like receptor recognizes bacterial DNA. Nature **408**:740–745.
25. **Hemmi, H., T. Kaisho, O. Takeuchi, S. Sato, H. Sanjo, K. Hoshino, T. Horiuchi, H. Tomizawa, K. Takeda, and S. Akira.** 2002. Small anti-viral compounds activate immune cells via the TLR7 MyD88-dependent signaling pathway. Nat. Immunol. **3**:196–200.
26. **Hofmann, C., V. Sandig, G. Jennings, M. Rudolph, P. Schlag, and M. Strauss.** 1995. Efficient gene transfer into human hepatocytes by baculovirus vectors. Proc. Natl. Acad. Sci. USA **92**:10099–10103.
27. **Hoshino, K., O. Takeuchi, T. Kawai, H. Sanjo, T. Ogawa, Y. Takeda, K. Takeda, and S. Akira.** 1999. Cutting edge: Toll-like receptor 4 (TLR4)-deficient mice are hyporesponsive to lipopolysaccharide: evidence for TLR4 as the LPS gene product. J. Immunol. **162**:3749–3752.
28. **Huser, A., M. Rudolph, and C. Hofmann.** 2001. Incorporation of decay-accelerating factor into the baculovirus envelope generates complement resistant gene transfer vectors. Nat. Biotechnol. **19**:451–455.
29. **Jarvis, D. L., and E. E. Finn.** 1995. Biochemical analysis of the N-glycosylation pathway in baculovirus-infected lepidopteran insect cells. Virology **212**:500–511.
30. **Kadowaki, N., S. Antonenko, J. Y. Lau, and Y. J. Liu.** 2000. Natural interferon alpha/beta-producing cells link innate and adaptive immunity. J. Exp. Med. **192**:219–226.
31. **Kawai, T., O. Takeuchi, T. Fujita, J. Inoue, P. F. Muhlradt, S. Sato, K. Hoshino, and S. Akira.** 2001. Lipopolysaccharide stimulates the MyD88-independent pathway and results in activation of IFN-regulatory factor 3 and the expression of a subset of lipopolysaccharide-inducible genes. J. Immunol. **167**:5887–5894.
32. **Krieg, A. M., and H. Wagner.** 2000. Causing a commotion in the blood: immunotherapy progresses from bacteria to bacterial DNA. Immunol. Today **21**:521–526.
33. **Krug, A., G. D. Luker, W. Barchet, D. A. Leib, S. Akira, and M. Colonna.** 2004. Herpes simplex virus type 1 (HSV-1) activates murine natural interferon-producing cells (IPC) through Toll-like receptor 9. Blood **103**:1433–1437.
34. **Kurt-Jones, E. A., L. Popova, L. Kwinn, L. M. Haynes, L. P. Jones, R. A. Tripp, E. E. Walsh, M. W. Freeman, D. T. Golenbock, L. J. Anderson, and R. W. Finberg.** 2000. Pattern recognition receptors TLR4 and CD14 mediate response to respiratory syncytial virus. Nat. Immunol. **5**:398–401.
35. **Kurt-Jones, E. A., M. Chan, S. Zhou, J. Wang, G. Reed, R. Bronson, M. M. Arnold, D. M. Knipe, and R. W. Finberg.** 2004. Herpes simplex virus 1 interaction with Toll-like receptor 2 contributes to lethal encephalitis. Proc. Natl. Acad. Sci. USA **101**:1315–1320.
36. **Lee, J., T. H. Chuang, V. Redecke, L. She, P. M. Pitha, D. A. Carson, E. Raz, and H. B. Cottam.** 2003. Molecular basis for the immunostimulatory activity of guanine nucleoside analogs: activation of Toll-like receptor 7. Proc. Natl. Acad. Sci. USA **100**:6646–6651.

37. **Lehtolainen, P., K. Tyynela, J. Kannasto, K. J. Airenne, and S. Y. Herttuala.** 2002. Baculoviruses exhibit restricted cell type specificity in rat brain: a comparison of baculovirus- and adenovirus-mediated intracerebral gene transfer in vivo. Gene Ther. **9**:1693–1699.
38. **Lematitre, B., E. Nicolas, L. Michaut, J. M. Reichhart, and J. A. Hoffmann.** 1996. The dorsoventral regulatory gene cassette spatzle/Toll/cactus controls the potent antifungal response in Drosophila adults. Cell **86**:973–983.
39. **Luckow, V. A., and M. D. Summers.** 1988. Signals important for high-level expression of foreign genes in Autographa californica nuclear polyhedrosis virus expression vectors. Bio/Technology **6**:47–55.
40. **Lund, J., A. Sato, S. Akira, R. Medzhitov, and A. Iwasaki.** 2003. Toll-like receptor 9-mediated recognition of herpes simplex virus-2 by plasmacytoid dendritic cells. J. Exp. Med. **198**:513–520.
41. **Lund, J., L. Alexopoulou, A. Sato, M. Karow, N. C. Adams, N. W. Gale, A. Iwasaki, and R. A. Flavell.** 2004. Recognition of single-stranded RNA viruses by Toll-like receptor 7. Proc. Natl. Acad. Sci. USA **101**:5598–5603.
42. **Matsuura, Y., R. D. Possee, H. A. Overton, and D. H. L. Bishop.** 1987. Baculovirus expression vector. The requirement for high level expression of proteins, including glycoproteins. J. Gen. Virol. **68**:1233–1250.
43. **Muzio, M., D. Bosisio, N. Polentarutti, G. Damico, A. Stoppacciaro, R. Mancinelli, C. vant Veer, G. Penton-Rol, L. P. Ruco, P. Allavena, and A. Mantovani.** 2000. Differential expression and regulation of Toll-like receptors (TLR) in human leukocytes: selective expression of TLR3 in dendritic cells. J. Immunol. **164**:5998–6004.
44. **Ozinsky, A., D. M. Underhill, J. D. Fontenot, A. M. Hajjar, K. D. Smith, C. B. Wilson, L. Schroeder, and A. Aderem.** 2000. The repertoire for pattern recognition of pathogens by the innate immune system is defined by cooperation between Toll-like receptors. Proc. Natl. Acad. Sci. USA **97**:13766–13771.
45. **Pieroni, L., D. Maione, and N. L. Monica.** 2001. In vivo gene transfer in mouse skeletal muscle mediated by baculovirus vectors. Hum. Gene Ther. **12**:871–881.
46. **Poltorak, A., X. He, I. Smirnova, M. Y. Liu, C. Van Huffel, X. Du, D. Birdwell, E. Alejos, M. Silva, C. Galanos, M. Freudenberg, P. Ricciardi-Castagnoli, B. Layton, and B. Beutler.** 1998. Defective LPS signaling in C3H/HeJ and C57BL/10ScCr mice: mutations in Tlr4 gene. Science **282**: 2085–2088.
47. **Rassa, J. C., J. L. Meyers, Y. Zhang, R. Kudaravalli, and S. R. Ross.** 2002. Murine retroviruses activate B cells via interaction with Toll-like receptor 4. Proc. Natl. Acad. Sci. USA **99**:2281–2286.
48. **Sandig, V., C. Hofmann, S. Steinert, G. Jennings, P. Schlag, and M. Strauss.** 1996. Gene transfer into hepatocytes and human liver tissue by baculovirus vectors. Hum. Gene Ther. **7**:1937–1945.
49. **Shoji, I., H. Aizaki, H. Tani, K. Ishii, T. Chiba, I. Saito, T. Miyamura, and Y. Matsuura.** 1997. Efficient gene transfer into various mammalian cells, including non-hepatic cells, by baculovirus vectors. J. Gen. Virol. **78**:2657–2664.
50. **Takeuchi, O., K. Hoshino, T. Kawai, H. Sanjo, H. Takeda, T. Ogawa, K. Takeda, and S. Akira.** 1999. Differential roles of TLR2 and TLR4 in recognition of gram-negative and gram-positive bacterial cell wall components. Immunity **11**:443–451.
51. **Takeuchi, O., and S. Akira.** 2001. Toll-like receptors: their physiological role and signal transduction system. Int. Immunopharmacol. **1**:625–635.
52. **Takeuchi, O., A. Kaufmann, K. Grote, T. Kawai, K. Hoshino, M. Morr, P. F. Muhlradt, and S. Akira.** 2000. Cutting edge: preferentially the R-stereoisomer of the mycoplasmal lipopeptide macrophage-activating lipopeptide-2 activates immune cells through a Toll-like receptor 2- and MyD88-dependent signaling pathway. J. Immunol. **164**:554–557.
53. **Tani, H., M. Nishijima, H. Ushijima, T. Miyamura, and Y. Matsuura.** 2001. Characterization of cell-surface determinants important for baculovirus infection. Virology **279**:343–353.
54. **Tani, H., C. K. Limn, C. C. Yap, M. Onishi, M. Nozaki, Y. Nishimune, N. Okahashi, Y. Kitagawa, R. Watanabe, R. Mochizuki, K. Moriishi, and Y. Matsuura.** 2003. In vitro and in vivo gene delivery by recombinant baculoviruses. J. Virol. **77**:9799–9808.
55. **Tokunaga, T., H. Yamamoto, S. Shimada, H. Abe, T. Fukuda, Y. Fujisawa, Y. Furutani, O. Yano, T. Kataoka, T. Sudo, N. Makiguchi, and T. Suganuma.** 1984. Antitumor activity of deoxyribonucleic acid fraction from Mycobacterium bovis BCG. I. Isolation, physicochemical characterization and antitumor activity. JNCI **72**:955–962.
56. **Tokunaga, T., T. Yamamoto, and S. Yamamoto.** 1999. How BCG led to the discovery of immunostimulatory DNA. Jpn. J. Infect. Dis. **52**:1–11.
57. **Underhill, D. M., A. Ozinsky, A. M. Hajjar, A. Stevens, C. B. Wilson, M. Bassetti, and A. Aderem.** 1999. The Toll-like receptor 2 is recruited to macrophage phagosomes and discriminates between pathogens. Nature **401**: 811–815.
58. **Wagner, H.** 2004. The immunobiology of the TLR9 subfamily. Trends Immunol. **25**:381–386.
59. **Yamamoto, M., S. Sato, H. Hemmi, K. Hoshino, T. Kaisho, H. Sanjo, O. Takeuchi, M. Sugiyama, M. Okabe, K. Takeda, and S. Akira.** 2003. Role of adaptor TRIF in the MyD88-independent Toll-like receptor signaling pathway. Science **301**:640–643.
60. **Zhang, D., G. Zhang, M. S. Hayden, M. B. Greenblatt, C. Bussey, R. A. Flavell, and S. Ghosh.** 2004. A Toll-like receptor that prevents infection by uropathogenic bacteria. Science **303**:1522–1526.
61. **Zheng, M., D. M. Klinman, M. Gierynska, and B. T. Rouse.** 2002. DNA containing CpG motifs induces angiogenesis. Proc. Natl. Acad. Sci. USA **99**:8944–8949.

THE JOURNAL OF BIOLOGICAL CHEMISTRY
Vol. 280, No. 33, Issue of August 19, pp. 29409–29419, 2005
Printed in U.S.A.

Ras-ERK MAPK Cascade Regulates GATA3 Stability and Th2 Differentiation through Ubiquitin-Proteasome Pathway*[S]

Received for publication, March 2, 2005, and in revised form, June 3, 2005
Published, JBC Papers in Press, June 23, 2005, DOI 10.1074/jbc.M502333200

Masakatsu Yamashita‡, Ryo Shinnakasu‡, Hikari Asou‡, Motoko Kimura‡, Akihiro Hasegawa‡, Kahoko Hashimoto§, Naoya Hatano¶, Masato Ogata¶, and Toshinori Nakayama‡‖

From the ‡Department of Immunology, Graduate School of Medicine, Chiba University, 1-8-1 Inohana Chuo-ku, Chiba 260-8670, the §Department of Life and Environmental Sciences and High Technology Research Center, Chiba Institute of Technology, Narashino, Tsudanuma, Chiba 275-0016, and the ¶Department of Biochemistry, Mie University School of Medicine, 2-174, Edobashi, Tsu, Mie 514-8507, Japan

Differentiation of naive CD4 T cells into Th2 cells requires protein expression of GATA3. Interleukin-4 induces STAT6 activation and subsequent GATA3 transcription. Little is known, however, on how T cell receptor-mediated signaling regulates GATA3 and Th2 cell differentiation. Here we demonstrated that T cell receptor-mediated activation of the Ras-ERK MAPK cascade stabilizes GATA3 protein in developing Th2 cells through the inhibition of the ubiquitin-proteasome pathway. Mdm2 was associated with GATA3 and induced ubiquitination on GATA3, suggesting its role as a ubiquitin-protein isopeptide ligase for GATA3 ubiquitination. Thus, the Ras-ERK MAPK cascade controls GATA3 protein stability by a post-transcriptional mechanism and facilitates GATA3-mediated chromatin remodeling at Th2 cytokine gene loci leading to successful Th2 cell differentiation.

In peripheral lymphoid organs, naive CD4 T cells that have recognized specific antigens differentiate into either one of two distinct helper T cell subsets, Th1 and Th2 cells (1). Upon antigen restimulation, Th1 cells produce large amounts of IFNγ[1] and direct cell-mediated immunity against intracellular pathogens. Th2 cells produce IL-4, IL-5, and IL-13 and are involved in humoral immunity and allergic reactions. The direction of Th cell differentiation depends on the types of cytokine in the environmental milieu (2, 3). Naive CD4 T cells stimulated with antigens in the presence of IL-12 differentiate into Th1 cells, whereas the presence of IL-4 drives differentiation into Th2 cells (4–6). IL-12-mediated activation of signal transducer and activator of transcription (STAT) 4 is crucial for Th1 cell differentiation, and IL-4-mediated STAT6 activation is important for Th2 cell development (7–9).

In addition to the cytokines mentioned above, activation of TCR-mediated signaling is also indispensable for both Th1 and Th2 cell differentiation. We reported that Th2 cell differentiation is highly dependent on the extent of TCR-mediated activation of the $p56^{lck}$, calcineurin, and Ras-ERK MAPK signaling cascade (10–12). In particular, inhibition of the activation of the Ras-ERK MAPK cascade caused a shift from Th2 to Th1 cell differentiation, suggesting that the direction of Th1/Th2 cell differentiation could be controlled by TCR-mediated activation of the Ras-ERK MAPK cascade (11, 13). On the other hand, Th1 cell development appeared to be regulated by another MAPK, c-Jun N-terminal kinase (14, 15).

Recently, several transcription factors that control Th1/Th2 cell differentiation were identified (8, 16). Among them, GATA3 appears to be a key factor for Th2 cell differentiation. GATA3 is selectively induced in developing Th2 cells after TCR stimulation in the presence of IL-4, and ectopic expression of GATA3 resulted in the induction of Th2 cell differentiation in the absence of STAT6 (17–20). GATA3 was found to be important for the maintenance of the Th2 phenotype (21, 22).

Th2 cell differentiation is accompanied by chromatin remodeling of the Th2 cytokine (IL-4/IL-5/IL-13) gene loci, *e.g.* hyperacetylation of histones H3 and H4 (23–25). Hyperacetylation of the IL-4 and IL-13 gene loci (23) and that of IL-5 gene locus (26) are highly dependent on the expression of GATA3. We described a precise map of the Th2-specific histone hyperacetylation within the Th2 cytokine gene loci, and we identified a 71-bp conserved GATA3-response element at 1.6 kbp upstream of the IL-13 locus (23). The GATA3-response element appears to play a crucial role for GATA3-mediated targeting and downstream spreading of core histone hyperacetylation within the IL-13 and IL-4 gene loci in developing $CD4^+$ Th2 and $CD8^+$ Tc2 cells (23, 27).

One of the major pathways of degradation of short lived regulatory proteins, including transcriptional factors, is through ubiquitin-mediated targeting and protein destruction in the 26 S proteasome. Protein ubiquitination is involved in a wide range of cellular processes, including cell cycle progression, signal transduction, transcriptional regulation, DNA re-

* This work was supported by grants from the Ministry of Education, Culture, Sports, Science and Technology (Japan), Grants-in-aid for Scientific Research Priority Areas Research 13218016 and 16043211, Scientific Research B 14370107, Scientific Research C 16616003 and 15790248, and Special Coordination Funds for Promoting Science and Technology, the Ministry of Health, Labor, and Welfare (Japan), the Program for Promotion of Fundamental Studies in Health Science of the Organization for Pharmaceutical Safety and Research (Japan), The Japan Health Science Foundation, Uehara Memorial Foundation, and Mochida Foundation. The costs of publication of this article were defrayed in part by the payment of page charges. This article must therefore be hereby marked "*advertisement*" in accordance with 18 U.S.C. Section 1734 solely to indicate this fact.

[S] The on-line version of this article (available at http://www.jbc.org) contains Fig. 1.

‖ To whom correspondence should be addressed: Dept. of Immunology (H3), Graduate School of Medicine, Chiba University, 1-8-1 Inohana, Chuo-ku, Chiba, 260-8670 Japan. Tel.: 81-43-226-2200; Fax: 81-43-227-1498; E-mail: tnakayama@faculty.chiba-u.jp.

[1] The abbreviations used are: IFNγ, interferon-γ; dn, dominant-negative; ERK, extracellular signal-regulated kinase; Erk2 sem., an active form of ERK2; KO, knock out (deficient); Tg, transgenic; Ub, ubiquitination; WT, wild type; TCR, T cell receptor; STAT, signal transducer and activator of transcription; IL, interleukin; PMA, phorbol 12-myristate 13-acetate; mAb, monoclonal antibody; ChIP, chromatin immunoprecipitation; MAPK, mitogen-activated protein kinase; MEK, MAPK/ERK kinase; siRNA, small interfering RNA; CHX, cycloheximide; GFP, green fluorescent protein; EGFP, enhanced GFP; hNGFR, human nerve growth factor receptor p75; FCS, fetal calf serum; E3, ubiquitin-protein isopeptide ligase.

pair, antigen presentation, and apoptosis (28–31). Emerging views suggest that various aspects of the immune system are controlled by ubiquitination (32). A well known example of the ubiquitin-dependent regulation in the immune system is the proteasome-dependent processing of peptides in antigen-presenting cells (33). It is also well known that lipopolysaccharide or proinflammatory cytokines such as IL-1 can induce activation of NF-κB through ubiquitination and subsequent degradation of the inhibitor of κB (34). However, a role for the ubiquitin-mediated regulation of Th1/Th2 cell differentiation has not been reported.

In the present study, we investigated the molecular targets of the Ras-ERK MAPK cascade that control chromatin remodeling of the Th2 cytokine gene loci and subsequent Th2 cell differentiation, and we found that the Ras-ERK MAPK cascade controls the stability of the GATA3 protein through the ubiquitin-proteasome pathway. Moreover, we demonstrated that the ubiquitination of GATA3 by Mdm2 is dependent on a ring finger domain.

EXPERIMENTAL PROCEDURES

Mice—C57BL/6 mice were purchased from SLC (Shizuoka, Japan). STAT6-deficient (KO) mice were kindly provided by Shizuo Akira (Osaka University, Osaka, Japan) (35). A T cell-specific H-ras dominant-negative (dnRas) transgenic (Tg) mouse with the *lck* proximal promoter was described elsewhere (11, 36). All mice used in this study were maintained under specific pathogen-free conditions.

Reagents—PD98059 (Calbiochem), cycloheximide (Calbiochem), MG132 (Sigma), and U0126 (Promega) were purchased.

Expression Plasmids and Transfection—Myc-tagged and FLAG-tagged GATA3 mutants (pCMV Tag 3B-GATA3 WT, dCT, dCF, and dZF), and GFP-fused GATA3 mutants (pEGFP-C1 GATA3 WT and pEGFP-C1 GATA3 dZF) were generated by PCR-based mutation. Myc-tagged wild type Mdm2, RING finger-deleted Mdm2 (pCMV Tag-3B-Mdm2 WT, dR), and $p19^{ARF}$ were generated in our laboratory. COS, 293T, and NIH3T3 cells were transfected using FuGENE reagent (Invitrogen) according to the manufacturer's protocol.

Cell Cultures and in Vitro T Cell Differentiation—CD4 T cells were purified using magnetic beads and an auto-MACS® sorter (Miltenyi Biotec), yielding a purity of >98%. The purified CD4 T cells (1.5×10^6) were stimulated for 2 days with immobilized anti-TCR mAb (H57–597, 3 μg/ml) in the presence of IL-2 (25 units/ml), IL-12 (100 units/ml), and anti-IL-4 mAb (11B11, 25% culture supernatant) for Th1-conditions or in the presence of IL-2 (25 units/ml), IL-4 (100 units/ml), and anti-IFNγ mAb (R4.6A2, 25% culture supernatant) for Th2− conditions. The cells were cultured for another 3 days in the presence of only the cytokines present in the initial culture. The numbers of Th1/Th2 cells were determined by using intracellular staining with anti-IL-4 and anti-IFNγ as described (10).

Retroviral Vectors and Infection—pMX-IRES-CAR (human coxsackie-adenovirus receptor) plasmid was generated from the pMX-IRES-GFP plasmid by replacing the EGFP gene with the CAR gene. The methods for the generation of virus supernatant and the infection were described previously (37). Infected cells were subjected to intracellular staining with anti-IL-4 and anti-IFNγ mAb or to cell sorting. To prepare large numbers of infected cells for immunoblotting, the pMX-IRES-CAR or pMXs-IRES-hNGFR vector was used, and the infected cells were enriched by auto-MACS® sorter with anti-CAR mAb (38) or anti-human NGFR (C40–1457; Pharmingen). cDNA encoding Erk2 sem was described previously (39). pMXs-Mdm2 dR-hNGFR was constructed by inserting Mdm2-dR into a multicloning site of pMXs-IRES-hNGFR. cDNA for human GATA3 or an active form of human Raf-1 (40) was inserted into a multicloning site of pMX-IRES-GFP.

Chromatin Immunoprecipitation (ChIP) Assay—ChIP was performed using the histone H3 assay kit (catalog number 17-245; Upstate Biotechnology, Inc.) as described previously (23). Semi-quantitative PCR was performed with DNA samples from 3 or 1×10^4 cells at 28 cycles. PCR products were resolved in an agarose gel and visualized by ethidium bromide. Images were recorded and quantified using ATTO L & S analyzer (ATTO, Tokyo, Japan). The primers used were described previously (23).

Immunoprecipitation and Immunoblotting—Purified CD4 T cells were stimulated with immobilized anti-TCR mAb for 2 days as described above, and nuclear extracts were prepared with an NE-PER™ nuclear and cytoplasmic extract reagent (catalog number 78833; Pierce) according to the manufacturer's protocol. The amount of GATA3, c-Maf, or α-tubulin was assessed by immunoblotting with anti-GATA3 mouse mAb (HG3–31; Santa Cruz Biotechnology, Santa Cruz, CA), anti-c-Maf rabbit antisera (M-153; Santa Cruz Biotechnology), or anti-α-tubulin mAb (DM1A; Lab Vision Corp.) as described previously (37). Anti-Mdm2 mAb (D-17; Santa Cruz Biotechnology), anti-E6-AP mAb (clone 20; BD Transduction Laboratories), anti-Itch mAb (clone 32; BD Transduction Laboratories), and anti-Cbl-b mAb (G-1; Santa Cruz Biotechnology) were used for immunoblotting. For transfectants, anti-FLAG mAb (M2; Sigma) and anti-Myc mAb (PL14; MBL) were used for immunoblotting.

For anti-ubiquitin blotting, COS cells were transfected with Myc-tagged GATA3 vectors (pCMV Tag 3B). Two days later, cells were treated with cycloheximide (100 μM) and U0126 (20 μM) in the presence or absence of the proteasome inhibitor MG132 (50 μM) for 2 h. The cells were then pelleted, resuspended in RIPA buffer, and lysed on ice for 30 min. Insoluble material was removed by centrifugation. The lysates were incubated with 5 μg of anti-Myc mAb (MBL, Japan) for 2 h at 4 °C. 50 μl of protein G-conjugated Sepharose (Amersham Biosciences) was then added and incubated for an additional 1 h. After removal of the supernatant, the beads were washed twice with RIPA buffer. The bound protein was eluted by adding 25 μl of SDS sample buffer and was subjected to immunoblot analysis using mAb specific for ubiquitin (FK2; MBL, Tokyo, Japan).

Northern Blotting—Total RNA (20 μg) was isolated from cultured cells using TRIzol reagent (Invitrogen), separated on a 1% formaldehyde gel, and transferred to a Nytran Plus membrane (Schleicher & Schuell). Probes for GATA3 and β-actin were generated by PCR using the primers described previously (37). The digoxigenin labeling and detection system (Roche Diagnostics) was used for visualization.

Pulse-Chase Experiment—Splenic CD4 T cells were stimulated for 2 days under Th2− conditions. The cells were washed, preincubated for 30 min in methionine/cysteine-free medium, and pulsed for 30 min with 200 μCi/ml [^{35}S]methionine/cysteine (ICN). Then the cells were washed twice with Dulbecco's modified Eagle's medium containing nonradioactive 5 mM L-methionine, 3 mM L-cysteine, and 0.25% FCS, and chased in the same medium in the presence of PMA (3 ng/ml) or PMA plus U0126 (20 μM). U0126 was used in the pulse-chase experiment because it is known to inhibit preactivated MEK as well (41).

In Vitro Ubiquitination Assay—*In vitro* ubiquitination assay was performed as described previously (42). In brief, 293T cells were transfected with FLAG-tagged GATA3, and 3 days later the cells were treated with MG132 for 2 h. Then the cells were lysed in RIPA buffer (2.5×10^6 cells/ml), and the cell lysates (250 μl) were subjected to immunoprecipitation with anti-FLAG or anti-GATA3 mAb. The immunoprecipitates were incubated for 2 h at 30 °C in 25 μl of reaction buffer containing 50 mM Tris-HCl (pH 8.0), 50 ng of recombinant mouse ubiquitin-activating enzyme, 500 ng of ubiquitin carrier protein, 5 μg of glutathione *S*-transferase-Ub, 1 mM dithiothreitol, 2 mM $MgCl_2$, and 4 mM ATP. After terminating the reaction by the addition of 2× SDS sample buffer, immunoblotting with anti-GATA3 or anti-FLAG mAb was performed. Recombinant mouse ubiquitin-activating enzyme, ubiquitin carrier protein, and glutathione *S*-transferase-Ub were kindly provided by Dr. Keiji Tanaka (Tokyo Metropolitan Institute for Medical Science, Tokyo, Japan).

siRNA—Introduction of siRNA into a T cell line TG40 was performed as described (43). In brief, 2 μl of TransIT-TKO transfection reagent (Mirus) was diluted in 50 μl of serum-free/antibiotic-free RPMI 1640 per well. Ten minutes later, 1 μl of 40 μM siRNA was added to the diluted transfection reagent and incubated for 30 min with gentle agitation. Then the siRNA solution was added to TG40 cultures containing 5×10^5 cells in 500 μl of medium per well in a 24-well plate. Three days after transfection, ubiquitination of GATA3 and the expression of Mdm2 protein were assessed by immunoblotting. Pre-designed siRNA for Mdm2 was purchased from Ambion (16704), and control siRNA was from Santa Cruz Biotechnology (sc-37007).

RESULTS

The Ras-ERK MAPK Cascade Controls Histone Hyperacetylation of the Th2− Cytokine Gene Loci—We reported that Th2 cell differentiation and certain Th2 responses are dependent on the extent of activation of the Ras-ERK MAPK cascade (11, 13). Hyperacetylation of the Th2 cytokine gene loci was highly dependent on the expression of GATA3 (23, 26). We present here further confirmation of the observations in chromatin remodeling of the Th2 gene loci. The generation of IL-4-produc-

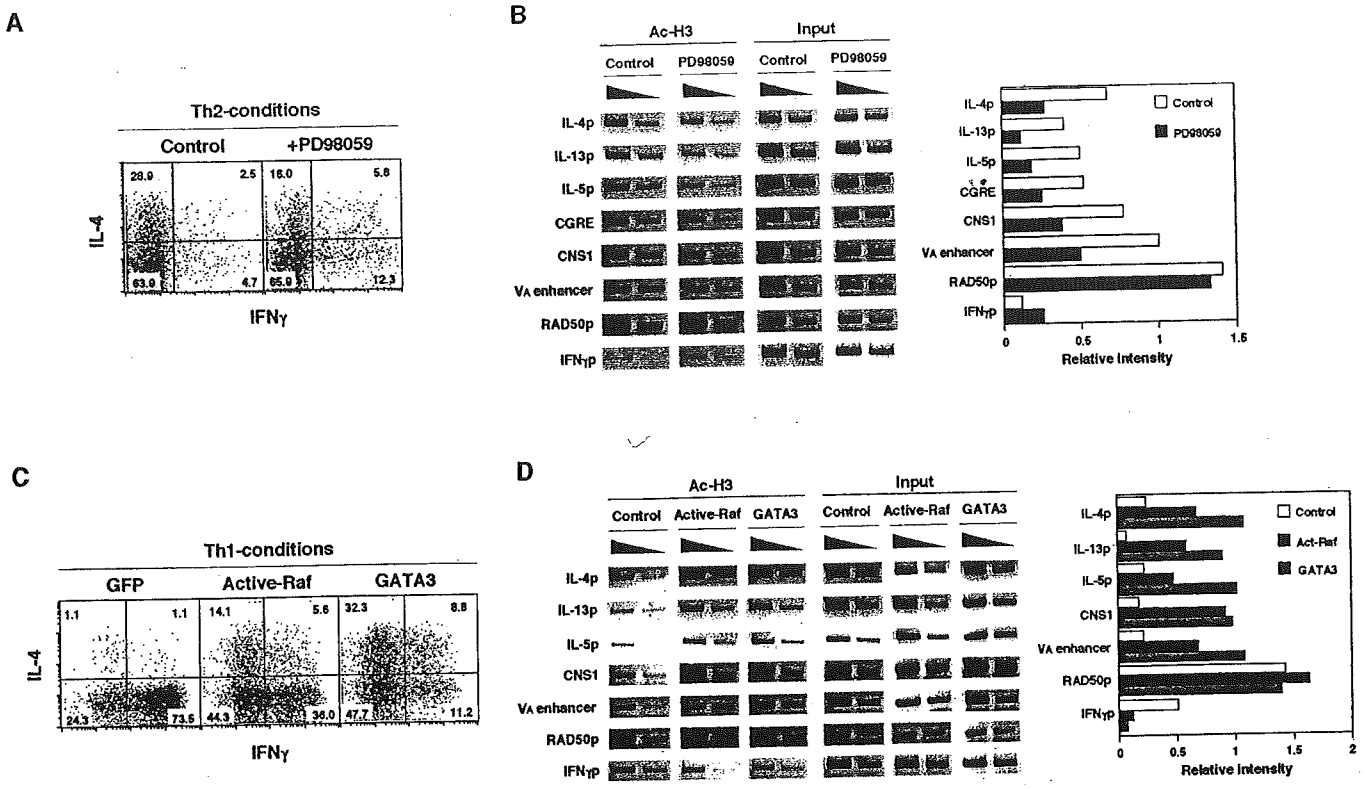

FIG. 1. **Activation of the ERK-MAPK cascade is required for GATA3-dependent histone H3 hyperacetylation of Th2 cytokine gene loci.** *A*, Th2 cell differentiation was inhibited by PD98059, a specific inhibitor of MEK. Freshly prepared splenic CD4 T cells were stimulated under Th2− conditions in the presence of PD98059 (30 μM) for 2 days. The cells were cultured for an additional 3 days and then stimulated with immobilized anti-TCR mAb. The numbers of Th1/Th2 cells were determined by intracellular staining with anti-IL-4 and anti-IFNγ. The *numbers* represent the percentages of cells in each quadrant. *B*, the effect of PD98059 on the histone H3 hyperacetylation. An aliquot of the cells cultured as in *A* were harvested on day 3, and the acetylation status of histone H3 in nucleosomes associated with the indicated regions was assessed by ChIP assay. An anti-acetylated histone H3 (K9, K14) antibody and specific primer pairs were used. Three independent experiments were performed, and similar results were obtained. Relative band intensities normalized by input DNA bands measured by a densitometer are shown in the *right panel*. *C*, expression of active Raf-induced IL-4 producing Th2 cells under Th1− conditions. Freshly prepared splenic CD4 T cells were stimulated under Th1− conditions and infected with retrovirus encoding active Raf or GATA3 bicistronically with EGFP on day 2. Three days later, the cells were stimulated with anti-TCR and were subjected to IL-4/IFNγ staining. *D*, histone H3 hyperacetylation on Th2 cytokine gene loci was induced by an active form of Raf-1 (*Active-Raf*) or ectopic expression of GATA3 in developing Th1 cells. GFP-positive infected CD4 T cells were enriched by cell sorting. *Control* represents mock vector virus infection. Acetylation status of histone H3 was determined by ChIP assay. Three independent experiments were done with similar results. Relative band intensities normalized by input DNA bands are shown in the *right panel*.

ing cells was substantially inhibited in the presence of a specific inhibitor of MEK (an ERK MAPKK), PD98059 (Fig. 1*A*). Fig. 1*B* shows that the acetylation levels of histones associated with the Th2 cytokine gene loci (IL-4 promoter, IL-13 promoter, IL-5 promoter, GATA3-response element, CNS1, and IL-4 V_A enhancer) were significantly reduced in the presence of PD98059. In the case of RAD50, there was no significant effect with PD98059 treatment, and with the IFNγ promoter (IFNγp) there was some enhancement in the acetylation. Under Th1 culture conditions, PD98059 exhibited no detectable inhibition of acetylation at the IFNγ promoter region (data not shown).

In addition, the effect of ectopic expression of an active form of Raf-1 (active-Raf) on the generation of Th1/Th2 cells was assessed. Significant numbers of IL-4-producing Th2 cells and a suppression of the generation of IFNγ-producing cells were observed in active Raf-infected cells stimulated under Th1− conditions (Fig. 1*C*). As a positive control, GATA3 infection was included, and in this case substantial levels of IL-4-producing cells with decreased numbers of IFNγ-producing cells were detected. Assessment of the acetylation status of histones in the active Raf-infected or GATA3-infected T cells defined by GFP expression on day 2 revealed significant increases in acetylation at the IL-4, IL-13, and IL-5 promoters and CNS1 and IL-4 V_A enhancer regions; however, the effect on the RAD50 promoter region was marginal (Fig. 1*D*). A significant decrease in the acetylation of the IFNγ promoter region was observed in the presence of active Raf. The levels of acetylation induced by active Raf infection were lower than those induced by GATA3. A possible explanation for this could be the limited expression of GATA3 in T cells cultured under Th1− conditions. Nevertheless, it is clear that the ERK-MAPK cascade controls GATA3-dependent histone hyperacetylation of the Th2 cytokine gene loci in developing Th2 cells.

Activation of the Ras-ERK MAPK Cascade Is Required for Stable Expression of GATA3 Protein in Developing Th2 Cells—GATA3 is a critical transcriptional factor for Th2 cell differentiation (17–19), and its expression is induced selectively under Th2− conditions. Here we demonstrate this in freshly prepared splenic CD4 T cells stimulated under Th1 and Th2 conditions (Fig. 2*A*, compare *lanes 1* and *3* and *lanes 2* and *4*). Treatment of Th2 condition cultures with PD98059 resulted in decreased protein expression of GATA3 (Fig. 2*A*, *lanes 5* and *6*). Similarly, the induction of GATA3 protein in dominant-negative Ras (dnRas) Tg T cells was significantly lower than that seen in the control, and this is consistent with the observation of impaired Th2 cell differentiation in dnRas Tg mice (11). A specific inhibitor for the p38 MAPK cascade (SB203580) did not affect the GATA3 expression in developing Th2 cells (data not shown). The activation of STAT6 is known to be critical for GATA3 transcription, and as expected, STAT6-deficient (STAT6 KO) CD4 T cells failed to induce GATA3 protein.

Concurrently, the transcriptional levels of GATA3 in T cells

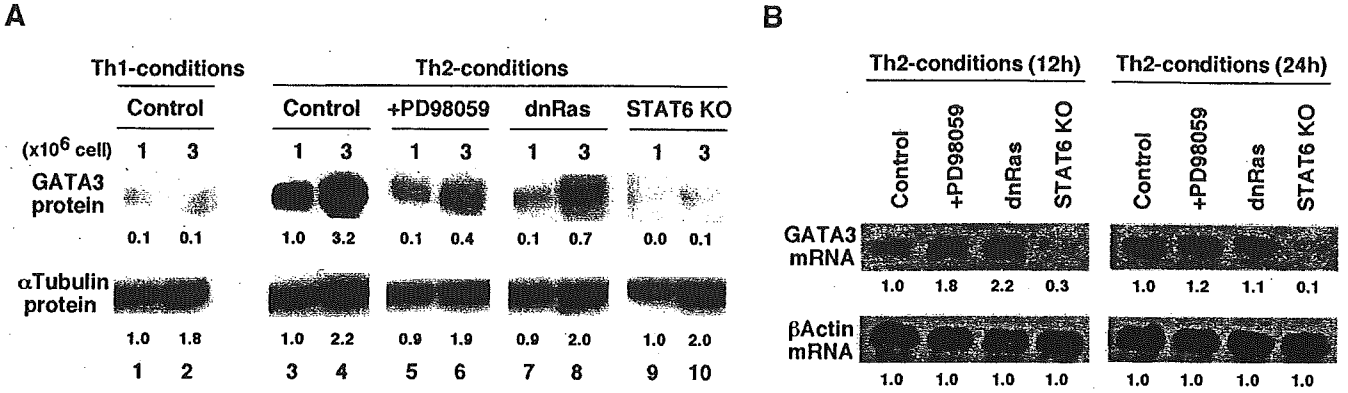

FIG. 2. **Activation of the ERK-MAPK cascade controls GATA3 protein expression without inhibiting transcription in developing Th2 cells.** *A*, ERK MAPK- and STAT6-dependent expression of GATA3 protein. Freshly prepared splenic CD4 T cells were stimulated under the indicated conditions for 2 days, and the expression of GATA3 protein in nuclei was assessed. CD4 T cells from T cell-specific dominant-negative H-Ras (dnRas) Tg mice and STAT6-deficient (STAT6 KO) mice were also used. The expression of α-tubulin was assessed as a control. A representative result from one of three independent experiments is shown. Arbitrary densitometric units normalized with α-tubulin bands are shown below each band. *B*, no effect of inhibition of the ERK-MAPK cascade on the transcriptional up-regulation of GATA3. Splenic CD4 T cells were stimulated under Th2− conditions for 12 and 24 h, and the expression levels of GATA3 mRNA were determined by Northern blot analysis. To examine the role for ERK-MAPK cascade activation, PD98059 (30 μM) and the CD4 T cells from dnRas Tg mice were used. Three independent experiments were performed with similar results. Arbitrary densitometric units are shown below each band.

cultured under Th2 conditions (12 and 24 h) as in Fig. 2*A* were assessed (Fig. 2*B*). The inhibition of activation of the Ras-ERK MAPK cascade by PD98059 or overexpression of dnRas transgene in T cells had no blocking effect on GATA3 mRNA expression. Rather, significant enhancement of GATA3 levels was detected at the 12-h time point. In contrast, GATA3 mRNA was not induced to significant levels in STAT6-deficient CD4 T cells, which is consistent with the lack of induced GATA3 protein.

Consequently, we sought to investigate further the consequence of the inhibition of ERK MAPK activation on the degradation of GATA3 protein. Splenic CD4 T cells were first stimulated under Th2− conditions for 2 days prior to being cultured without IL-4 or immobilized anti-TCR mAb for various time periods (chase) in either the presence or absence of another specific MEK inhibitor (U0126), which is also effective on activated MEK (Fig. 3, *A* and *B*). Under normal culture conditions with 10% FCS, the levels of GATA3 protein remained elevated over 12 h but then they declined significantly at 24 h. In the presence of U0126, significant reduction of GATA3 protein was observed at the 6- and 12-h time points, and the protein was virtually undetectable after a 24-h chase (Fig. 3*A*). U01126 treatment did not affect the level of another Th2-specific transcription factor, c-Maf. Under culture conditions with low levels of FCS (0.25%), where decreased levels of background stimulation of the MAPK cascades were detected (data not shown), a gradual decrease in GATA3 protein was seen and a modest rescue by the presence of PMA was observed (Fig. 3*B*). In the presence of U0126, the loss of GATA3 protein was dramatic, and GATA3 was barely detectable at the 12- and 24-h time points.

As an alternative means to assess the effect of ERK MAPK on the stability of the GATA3 protein, we performed pulse-chase experiments to follow the degradation of GATA3, and we found that the amount of ^{35}S-labeled nascent GATA3 protein was degraded very rapidly in the presence of U0126 (Fig. 3*C*). These results clearly demonstrate that rapid degradation of GATA3 occurs when activation of ERK MAPK is inhibited.

As a more direct test of the requirement for the activation of ERK MAPK to stabilize GATA3 in developing Th2 cells, we introduced an active form of ERK2 (Erk2 sem) (39) or a dominant-negative form of ERK2 (dnErk2) (44) into developing Th2 cells (Fig. 3*D*). As anticipated, GATA3 protein was significantly retained in cells infected with ERK2 sem, whereas the expression of dnERK2 significantly enhanced its degradation. Thus, the stability of GATA3 protein in developing Th2 cells appears to be highly dependent on the activation of the Ras-ERK MAPK cascade.

GATA3 Is Rapidly Degraded through the 26 S Proteasome Pathway—It would seem very likely that the proteasome pathway would be involved. To determine whether the 26 S proteasome is involved with the rapid degradation of the GATA3 protein, the effect of a proteasome inhibitor MG132 was examined. COS cells were transfected with Myc-tagged GATA3 and treated with cycloheximide (CHX) to inhibit protein synthesis in the presence or absence of MG132 for 1 or 2 h. Myc-tagged GATA3 was predominantly expressed in the nucleus, and after CHX treatment it was degraded rapidly in the absence of MG132 (Fig. 4*A*, *left panel*). In contrast, in the presence of MG132, there was a dramatic increase in the amount of Myc-tagged GATA3 protein in both nuclear and cytoplasmic fractions (Fig. 4*A*, *right panel*). Moreover, in developing Th2 cells GATA3 protein was degraded rapidly in the presence of CHX, and the degradation was inhibited by MG132 (Fig. 4*B*). In addition, another proteasome inhibitor lactacystin was tested in primary T cells for its ability to affect the degradation of GATA3, and a significant blocking of the degradation of GATA3 was observed (Fig. 4*C*). Collectively, these results point to the involvement of the 26 S proteasome pathway in the degradation of GATA3.

The C-terminal Region of GATA3 Including the Zinc Finger Domain Is Critical for Proteasome-dependent Degradation—In an attempt to map the target region of GATA3 that is critical for proteasome-dependent degradation, we prepared several truncated GATA3 mutants of the N-terminal region, which contains many lysine residues that can be ubiquitinated (Fig. 4*D*). Myc-tagged wild type (WT), dCT, dCF, and dZF constructs were transfected into COS cells, and the expression levels of GATA3 were assessed after treatment with MG132 (Fig. 4*E*). In comparison to wild type GATA3, there was essentially no difference in the pattern of disappearance of either the dCT or dCF mutant forms from nuclear fractions following CHX treatment, or in the retention of GATA3 protein by MG132 treatment. In the cytosol fraction of transfectants without drug treatment, slightly increased levels of protein were detected with dCT and dCF mutants, but the levels after treatment with MG132 were indistinguishable (Fig. 4*E*, *lower panels*). In sharp contrast, large amounts of dZF mutant protein were detected in